### Title

Experimental and Computational Studies of Carbon–Carbon Bond Formation via Ketonization and Aldol Condensation over Site-Isolated Zirconium Catalysts




### Journal

ACS Catalysis, 10(8)

### ISSN

2155-5435



### Authors

Shylesh, Sankaranarayanapillai
Bettinson, Lance A
Aljahri, Ahmed
et al.



### Publication Date

2020-04-17

### DOI

10.1021/acscatal.9b05176

Peer reviewed

# Experimental and Computational Studies of Carbon-Carbon Bond Formation via Ketonization and Aldol Condensation over Site-Isolated Zirconium Catalysts

Sankaranarayanapillai Shylesh,[‡,a] Lance A. Bettinson, [‡,a,b], Ahmed Aljahri,[a] Martin Head-Gordon,[a,c] and Alexis T. Bell*[a,b]

[a]Chemical Sciences Division, Lawrence Berkeley National Laboratory, Berkeley, CA 94720

[b]Department of Chemical and Biomolecular Engineering, University of California, Berkeley, California 94720

[c]Department of Chemistry, University of California, Berkeley, California 94720

Submitted to
ACS Catalysis

[‡]Contributed to the work equally

*To whom correspondence should be addressed

**Abstract**

We report here the preparation and investigation of isolated Zr centers supported on a high surface area silica for the conversion of carboxylic acids to internal ketones by ketonic decarboxylation (ketonization) and the aldol condensation of ketones to dimeric enones. Catalysts were synthesized by the grafting of $Cp_2ZrCl_2$ on the surface of amorphous silica. The connectivity of Zr was characterized by XRD, UV-Vis, and Raman spectroscopy. For the lowest Zr loading, Zr is present predominantly as isolated monomeric species. As the Zr loading is increased, a progressively larger fraction of Zr forms oligomeric species and $ZrO_2$ nanoparticles. Measurements of catalytic activity show that the turnover frequency for carboxylic acid ketonic decarboxylation reaction and aldol condensation of ketones decreases monotonically with increasing Zr loading. An H/D kinetic isotope effect was not observed over isolated Zr catalysts, suggesting that α-H abstraction is not the rate-determining step rather C-C bond forming may be rate limiting for both reactions. This conclusion is supported by computational modeling of the reaction mechanism. The proposed catalytic cycle for ketonization proceeds via a β-keto acid intermediate on isolated Zr sites that are always coordinatively saturated, with C-C bond formation as the rate-limiting step. C-C bond formation is also rate-determining for aldol condensation, with an apparent activation energy that is in good agreement with experiment if the resting state is a saturated ≡ZrOH site with two adsorbed ketone molecules.

## Introduction

Biomass and biomass-derived products are an attractive source of renewable carbon for producing chemicals and fuels.[1,2] A significant drawback to using these feedstocks is their high content of oxygen. For example, bio-oil produced by fast pyrolysis of biomass contains a high fraction of acids, alcohols, aldehydes, esters, phenolics, and other oxygenates.[3,4] Of these compounds, the largest fraction comprises low molecular weight carboxylic acids, aldehydes, and ketones (R-COOH, R-CHO, R-CO-R). Carboxylic acids can also be produced by fermentation of sugars.[5] Because of their low molecular weight and high oxygen content, these compounds cannot be used as fuels without being upgraded to products containing more carbon atoms and fewer oxygen atoms.[6–10]

An attractive approach for removing oxygen from biomass-derived carboxylic acids is ketonic decarboxylation (ketonization).[11,12] This reaction condenses two carboxylic acid molecules, eliminating 75% of the oxygen in the reactants to produce a linear ketone with 2n-1 carbon atoms, $CO_2$, and $H_2O$.[11] The alkanone produced by ketonic decarboxylation can undergo subsequent aldol condensation, thereby further increasing the chain length of the product and its energy density via the removal of oxygen as water.[13] While ketonic decarboxylation is conventionally promoted by homogeneous base catalysts, such as NaOH or KOH, catalyst separation from the reaction mixture is difficult and catalyst disposal is expensive.[14]

Previous studies have shown that bulk and dispersed metal oxides are promising heterogeneous catalysts for ketonic decarboxylation and aldol

condensation because they contain Lewis acid-Brønsted base pairs on their surface.[11] Oxides with a high lattice energy, such as $TiO_2$ or $ZrO_2$, are particularly active and selective for C-C bond formation because carboxylic acids or aldehydes can adsorb at Lewis-acidic Ti or Zr sites. The resulting adsorbate can then undergo abstraction of the α-proton at an adjacent Brønsted-basic oxygen sites.[9,15–20]

The purpose of this study was to elucidate the role of local coordination and connectivity of supported Zr sites on the gas-phase, ketonic decarboxylation of carboxylic acids and aldol condensation of ketones. Catalysts were prepared by impregnation of the support with a metal alkoxide precursor and then characterized by XRD, Raman and UV-Vis spectroscopy. Since we were particularly interested in investigating the properties of isolated Zr structures, well-defined active sites were obtained either by the grafting an organometallic Zr precursor onto a silica support or by incorporating Zr into the framework of a mesoporous silica. We observed that isolated, tetrahedrally coordinated Zr species (≡Zr-OH) are more active for ketonic decarboxylation of carboxylic acids and aldol condensation of ketones than tetrahedrally coordinated Zr dimer species and octahedrally coordinated $ZrO_2$ nanoparticles dispersed on silica. Based on this finding, we focused attention on the kinetics of ketonic decarboxylation and aldol condensation occurring on isolated ≡Zr-OH species. The mechanism by which these reactions proceed was probed both experimentally and by computational quantum chemistry calculations.

## 2.0. Experimental methods

### 2.1. Catalyst Synthesis

Zirconium was grafted onto a silica support using the following procedure. One gram of amorphous silica (Silicycle, surface area: 500 $m^2$ $g^{-1}$) was dried in vacuum at 373 K for 24 h, or pretreated at 1023 K for 5 h, and then stored in vacuum prior to use. Zr was introduced onto the silica surface either by grafting $Cp_2ZrCl_2$ (Aldrich, 97%) dissolved in toluene (Alfa Aesar, anhydrous 99.8% pure) or by impregnation with a toluene solution of $Zr(O^iPr)_4$ (Aldrich, 99.999%). These catalysts are referred to as *x*ZrCp/$SiO_2$ and *x*ZrPr/$SiO_2$, respectively, where *x* denotes the dispersion of zirconium (atoms $nm^{-2}$). A similar synthesis procedure was utilized for the synthesis of titanium-silica and tin-silica catalysts using $Cp_2TiCl_2$ and $(CH_3)_2SnCl_2$ as the respective metal precursors. All impregnated and grafted catalysts were dried at 393 K for 12 h and calcined in 100 $cm^3$ $min^{-1}$ of air (Praxair) for 823 K for 6 h. A zirconium dimer complex, $[(i\text{-}PrCp)_2ZrH(\mu\text{-}H)]_2$ was also prepared according to literature procedures.[18]

### 2.2. Catalyst Activity

Reaction rates were measured using a 6.35 mm OD quartz reactor containing an expanded section (~12.7 mm OD, ~20 mm length). A plug of quartz wool placed below the catalyst bed to hold the powder in place. The catalyst bed temperature was measured with a K-type thermocouple sheathed in a quartz capillary placed in direct contact with the catalyst bed. Prior to reaction, the catalyst was heated to the reaction temperature at a rate of 2 K $min^{-1}$ in pure He (Praxair,

99.999%) flowing at 100 $cm^3min^{-1}$ at STP. A filled 1 mL syringe connected to a syringe pump (Cole-Palmer, 74900 series) was used to inject propanoic acid or propan-2-one into a heated port through which helium was flowed continuously. All experiments were carried out at a total gas pressure of 1 atm. The total gas flow rate was typically 100 $cm^3$ $min^{-1}$ at STP. Under these conditions, the conversion of carboxylic acids or propan-2-one was less than 20%. Reaction products were analyzed using an Agilent 6890N gas chromatograph containing a bonded and cross-linked (5%-phenyl)-methylpolysiloxane capillary column (Agilent, HP-1) connected to a flame ionization detector (FID). The rate of product formation per Zr atom, or turnover frequency (TOF) was calculated by dividing the measured rate of reaction per gram of catalyst by the measured amount of Zr per gram of catalyst.

### 2.3. Characterization

The metal content of the catalysts was determined by inductively coupled plasma optical emission spectroscopy (ICP-OES) at Galbraith Laboratories (Knoxville, TN). Nitrogen adsorption isotherms were performed using a Micromeritics Gemini VII surface area and pore volume analyzer. The specific surface area and pore size were calculated using the Brunauer-Emmet-Teller (BET) equation and Barrett-Joyner-Halenda (BJH) equations. Raman spectra were acquired at ambient conditions using a confocal Raman microscope (LabRam HR, Horiba Jobin Yvon) equipped with a 532 nm HeNe laser operated at a power of 50 mW. Diffuse reflectance UV-Vis spectra were acquired using a Fischer Scientific EVO 300 spectrometer equipped with a Praying Mantis

reflectance chamber. Spectra were referenced to the diffuse reflectance spectrum of Teflon.

### 2.3. Computational methods.

The active site for ketonization and aldol condensation was represented by a cluster comprised of an isolated ZrOH group incorporated into the corner of silsesquioxane, as shown in Figure 1. This model has previously been used to investigate aldol condensation on isolated TiOH groups supported on silica,[20] and more generally silsesquioxanes have been used to as molecular models of silica-grafted metal hydroxo and oxo species.[21] Geometry optimization of the intial structure preceded all calculations of adsorbed species. The structure of each adsorbed species on the optimized active site was then further optimized by relaxing the metal center, all atoms in its first coordination sphere, and the hydrogen of the terminal hydroxyl group. The vibrations of the converged species were then determined. These calculations were done using the ωB97X-D functional[22,23] and the def2-SVP basis set and the def2-ECP for Zr (ωB97X-D/def2-SVP level of theory).[24] The resulting Hessian matrix output with zero negative eigenvalues (i.e. zero imaginary frequencies) confirmed that a given structure was at an energetic minimum. Structural convergence was followed by higher accuracy single-point energy calculations at the ωB97M-V/def2-TZVP level of theory.[24,25]

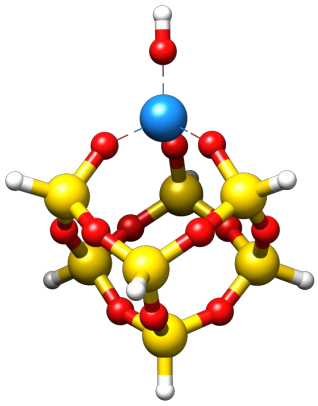

**Figure 1. Cluster model of isolated M-OH site on silica support.** White, red, and yellow spheres represent H, O, and Si atoms, respectively. The blue sphere represents the Zr metal site.

Estimates of the transition state structures occurring between reactant and product states were obtained using the freezing string method.[26] These estimates were then refined to transition structures at the ωB97X-D/def2-SVP level of theory. Similar to geometry optimization of reaction intermediates, transition structures were confirmed by the presence of one negative eigenvalue in the Hessian matrix corresponding to motion in a single direction (the reaction coordinate). Visualization of the corresponding imaginary frequency was used to identify a vibrational mode in the direction of bond formation. All calculations were performed using the Q-Chem software package.[27]

Enthalpies and entropies at the reaction temperature were determined by calculating the zero-point vibrational energy and the temperature corrections to the enthalpy using the quasi-rigid rotor harmonic oscillator (q-RRHO) approach proposed by Grimme.[28] This approach replaces the vibrational entropy and enthalpy for low frequency modes (< 100 $cm^{-1}$) by an interpolation between the rigid rotor harmonic oscillator (RRHO) vibrational values and free-rotor rotational

values. The turnover frequencies (TOFs) of the catalytic cycles were predicted using Kozuch's model of a catalytic cycle, which uses transition state theory to predict the TOF from estimates of the Gibbs free energy and enthalpy for all reaction intermediates and transition states, weighted by appropriate reactant and product partial pressure contributions.[29,30]

We used this model to determine the rate limiting transition structures and most abundant surface intermediates for both ketonization and aldol condensation. Where applicable, we performed a degree of rate control analysis[31,32] to determine dominant intermediate states in the reaction mechanism. These were then used to predict experimentally observed activation energies from the free energies of reaction intermediates following a procedure described by Mao and Campbell.[33]

## 3. Results and Discussion

### 3.1. Catalyst Characterization

The properties of each catalyst are shown in Table 1. The surface area of the $Cp_2ZrCl_2$ grafted silica sample is very similar to that of the silica support at low Zr loadings and decreases progressively with increasing weight loading of Zr on the silica support. We note that a part of this loss is apparent and is associated with the increasing mass of the deposited Zr relative to that of the silica support.

**Table 1.** Chemical and textural properties of Zr containing silica samples

| Sample | Zr content (wt.%) | BET surface area ($m^2g^{-1}$) | TOF ($10^{-4}$, $s^{-1}$) |
|---|---|---|---|
| 0.07ZrCp/$SiO_2$ | 0.61 | 495 | 3.2 |
| 0.1ZrCp/$SiO_2$ | 0.82 | 490 | 3.3 |
| 0.1ZrCp/$SiO_2$[a] | 0.82 | 482 | 7.3 |
| 0.5ZrCp/$SiO_2$ | 3.85 | 435 | 2.5 |
| 0.7ZrCp/$SiO_2$ | 4.30 | 413 | 1.5 |
| 1.0ZrCp/$SiO_2$ | 6.10 | 385 | 0.5 |
| 0.1ZrPr/$SiO_2$ | 0.86 | 473 | 2.1 |
| $SiO_2$ | - | 500 | 0 |

[a] Sample prepared on silica calcined at 1023 K prior to grafting with $Cp_2ZrCl_2$. Reaction conditions: T = 573 K, $P_{Total}$ = 1 atm, $Q_{Total}$ = 100 $cm^3$ $min^{-1}$, $P_{acid} \approx 0.2$ kPa, $M_{Cat}$ = 0.1 g.

Literature XANES and EXAFS analysis of Zr dispersed on silica derived from $Cp_2ZrCl_2$ and $Zr(O^iPr)_4$ showed that Zr forms in coordinatively unsaturated, tetragonal structures.[18] We further probed the coordination and connectivity of Zr by Raman and UV-Vis spectroscopy. Raman spectra of the silica support and various *x*ZrCp/$SiO_2$ samples are shown in Figure S1. The spectrum of the support exhibits peaks at 485 $cm^{-1}$ and 975 $cm^{-1}$ attributable to the stretching vibrations of four-membered siloxane linkages (Si-O-Si) and surface silanol groups ($O_3$Si-OH), respectively.[20] For loading of up to 0.1 Zr $nm^{-2}$, the spectrum of ZrCp/$SiO_2$ is indistinguishable from that of silica because of the low weight loading of Zr. Samples with higher Zr loadings exhibit the characteristic peaks of tetragonal zirconia at 600 $cm^{-1}$ and 800 $cm^{-1}$ due to $A_g$ vibrations of Zr-O-Zr bonds.[34] Although

XRD patterns do not show the presence of bulk oxides at any Zr loading levels, the Raman spectra suggest that a fraction of the Zr is present as $ZrO_2$ nanoparticles, possibly in particles smaller than 5 nm in diameter for loadings of more than 0.5 Zr atoms $nm^{-2}$.

The UV-Vis edge energy of *x*ZrCp/$SiO_2$ prepared with different Zr surface densities is shown in Figure 2 together with those of model compounds. The observed decrease in the edge energy of xZrCp/$SiO_2$ with increasing Zr surface density is attributable to an increase in the connectivity of Zr atoms. These results suggest that, at low Zr loading (0.1 Zr atoms $nm^{-2}$), Zr exists as isolated tetrahedral structures, at intermediate Zr loadings (0.5 Zr atoms $nm^{-2}$), possibly as dimeric or oligomeric species, and at high loadings (1.0 Zr atoms $nm^{-2}$), as bulk-like $ZrO_2$ structures. The trend in Zr speciation with increasing Zr surface density is supported by measured edge energies for the model compounds $Cp_2ZrCl_2$ (isolated Zr atoms) and $[(i\text{-}PrCp)_2ZrH(\mu\text{-}H)]_2$ (isolated Zr dimers) and for bulk $ZrO_2$.

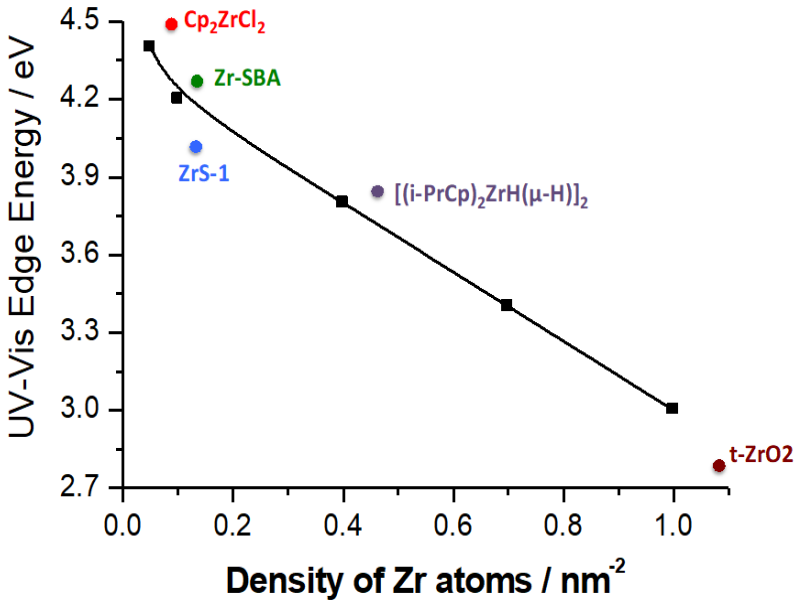

**Figure 2.** UV-Vis edge energies of *x*ZrCp/$SiO_2$ as a function of Zr surface density and Zr-containing model compounds.

### 3.2. Ketonization of propanoic acid

The catalytic activity of silica-supported zirconia was evaluated for the ketonic decarboxylation of propanoic acid at 573 K. Experiments were conducted under conditions of differential conversion (< 2%) so that catalyst deactivation and secondary condensation could be minimized. The only product observed under the conditions investigated was pentan-3-one. The rate of formation of the product was zero order in the partial pressure of propanoic acid for partial pressures between 0.1 kPa and 0.4 kPa (Figure S2). Control experiments with silica displayed no catalytic activity, indicating that surface-grafted zirconium sites are responsible for the observed catalytic activity.

The dependence of the specific activity of ZrCp/$SiO_2$ on the Zr loading is shown in Figure 3. As the surface density of Zr increases, the turnover frequency decreases monotonically. The catalyst prepared with a low surface concentration of zirconium (0.1 Zr $nm^{-2}$) is approximately six times more active than that prepared with 1.0 Zr $nm^{-2}$, whereas the activity of the catalyst prepared with a high zirconium, such as 2.0 Zr $nm^{-2}$ in negligible. The high activity of 0.1ZrCp/$SiO_2$ suggests that isolated tetrahedrally coordinated Zr sites are more active than Zr atoms in clusters.

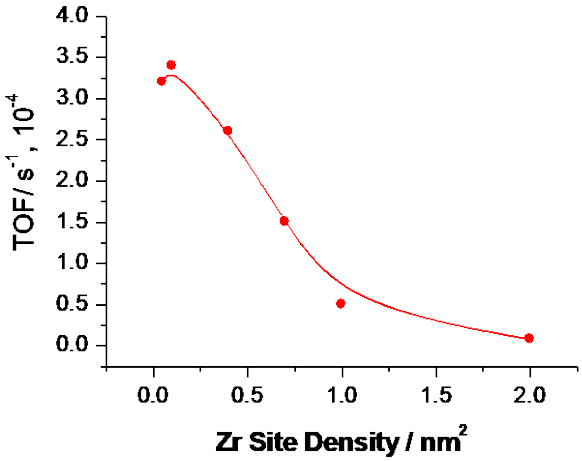


**Figure 3.** Effect of Zr site density in the activity of *x*ZrCp/$SiO_2$ catalysts for ketonization of propanoic acid. Reaction conditions: T = 573 K, $P_{Total}$ = 1 atm, $Q_{Total}$ = 100 $cm^3$ $min^{-1}$, $P_{acid} \approx$ 0.2 kPa, $M_{Cat}$ = 0.1 g.

FT-IR spectra of adsorbed $CH_3CN$ were acquired as a function of temperature to probe the strength of Lewis and Brønsted acidic sites. As shown in Figure S3, the peaks observed at 2315 $cm^{-1}$ and 2290 $cm^{-1}$ correspond to the $\nu$(CN) mode of $CH_3CN$, N-coordinated to Zr split by the coupling with the $\nu$(CC) + $\delta_{sym}(CH_3)$ combination, while the peak at 2260 $cm^{-1}$ corresponds to physisorbed or H-bonded $CH_3CN$ associated with surface hydroxyl groups.[35] A strong absorption band is not observed in the region of 2200-2050 $cm^{-1}$, characteristic of $\nu$(CN) modes of $CH_2CN^-$ species and polymeric anions such as $[CH_3C(NH)CHCN]^-$, suggesting the absence of strongly Lewis basic sites on ZrCp/$SiO_2$.[36]

The data presented in Figure S3 show that $CH_3CN$ desorbs at a lower temperature from Zr oligomers (1.0 Zr $nm^{-2}$) than from isolated ≡Zr-OH species (0.1 Zr $nm^{-2}$). These results suggest that more highly coordinated Zr sites are less

Lewis acidic than isolated four-coordinated Zr sites, from which we infer that the adsorption of propanoic acid via binding of the carbonyl group with the Lewis acid center will be stronger with isolated Zr atoms sites than with Zr atoms that are part of a ZrOx oligomer. Thus we attribute the decrease in the ketonization activity for catalysts with higher Zr site densities to the formation of ZrOx dimers and oligomers, in a manner similar to what we previously reported for aldol condensation on TiOx species.[20]

To obtain additional support for the above hypothesis, the silica support was calcined at progressively higher temperatures in order to achieve spatial separation of the silanol groups prior to grafting $Cp_2ZrCl_2$ onto the support. $^{29}Si$ MAS NMR indicates that silica pretreated at 373 K and 1023 K possess nearly 4 and 1.6 SiOH $nm^{-2}$, respectively.[37] As shown in Table 1, the TOF of $0.1ZrCp/SiO_2$ catalyst prepared on silica pretreated at 1023 K is roughly twice as high as that for $0.1ZrCp/SiO_2$ prepared on silica pretreated at 373 K. This inverse correlation between the activity and the density of support silanol groups supports the idea that isolated ZrOH centers are most active for carboxylic acid ketonization. By contrast, Zr catalysts synthesized by incipient wetness impregnation using $Zr(O^iPr)_4$, showed a much lower TOF than those prepared by grafting $Cp_2ZrCl_2$ for similar Zr loadings (Table 1). These findings are consistent with previous studies done on titania dispersed on silica, which show that a metal alkoxide precursor such as $Ti(O^iPr)_4$ reacts with surface silanols to form dinuclear Ti complexes.[38]

Further experiments were undertaken to obtain information about the mechanism of the reaction. The first of these involved examination of the inhibiting

effects of ketone, $CO_2$ and water, the products formed during the ketonization of propanoic acid over $ZrCp/SiO_2$. We also explored the effect of co-feeding pyridine, a Lewis base expected to inhibit the reaction. As illustrated in Figure 4, co-feeding pyridine or water with the reactants produced an approximately two-fold decrease in the rate of ketone formation. However, co-feeding $CO_2$ decreased the rate of ketone formation only marginally. These results show that activity of $0.1ZrCp/SiO_2$ for the ketonization of propanoic acid decreases in the order: $H_2O > C_6H_5N > CO_2$. The data in Figure 4 also show that upon removal of $CO_2$ from the feed, the activity returned to that observed prior to the addition of this compound; however, in the cases of water and pyridine addition, the original activity was only partially restored. The incomplete recovery of activity after the removal of pyridine or water from the feed suggests that Lewis acidic sites are more relevant than the Brønsted basic sites (e.g., Zr-OH) for the ketonization of propanoic acid over isolated sites of Zr supported on $SiO_2$.

To confirm that isolated ≡Zr-OH sites only contain Lewis acidic sites, and not Bornsted acid sites, we acquired IR spectra of adsorbed pyridine on $0.1ZrCp/SiO_2$. Prior work has shown that IR peaks at 1445, 1575, and 1605 $cm^{-1}$ are attributable to strong Lewis acid sites; a peak at 1490 $cm^{-1}$, to a combination of Lewis and Brønsted acid sites; and peaks at 1540 and 1640 $cm^{-1}$, to Brønsted acid sites.[39] The IR spectra shown in Figure S4 indicates that $0.1ZrCp/SiO_2$ possess pyridine bonded to strong Lewis acid sites (peaks at 1445, 1575, and 1605 $cm^{-1}$) and no evidence for pyridine interacting with Brønsted acid sites.

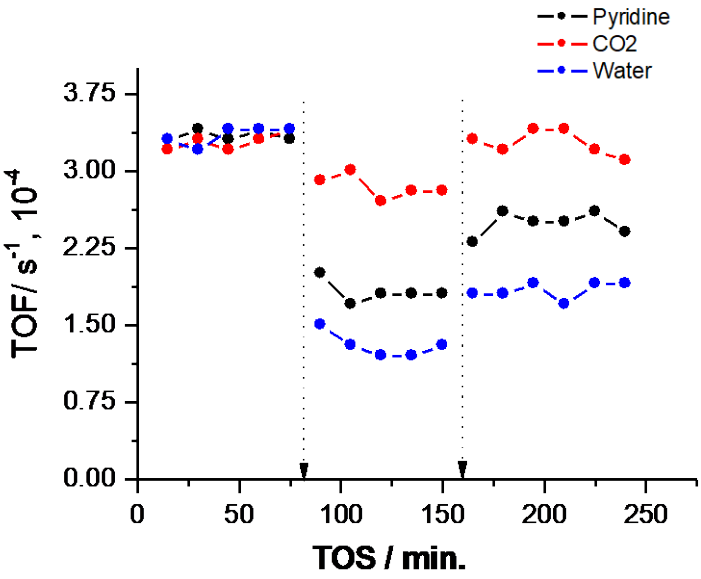


**Figure 4.** Poisoning experiments conducted over 0.1ZrCp/$SiO_2$ catalysts in the ketonic decarboxylation of propanoic acid. Dotted lines represent the time at which 10 wt.% of the poisoning agent was co-fed together with propanoic acid in the gas stream. Reaction conditions: T = 573 K, $P_{Total}$ = 1 atm, $Q_{Total}$ = 100 $cm^3$ $min^{-1}$, $P_{acid}$ ≈ 0.2 kPa, $M_{Cat}$ = 0.1 g.

In situ IR spectroscopy was used to probe the form in which a carboxylic acid interacts with isolated Zr sites on 0.1ZrCp/$SiO_2$. As seen in Figure 5, upon passing pulses of acetic acid over 0.1ZrCp/$SiO_2$ at 373 K, a peak was observed at 1745 $cm^{-1}$ for acetic acid adsorbed on the silanol groups of silica, and a second peak was observed at 1680 $cm^{-1}$ attributable to the interaction of -C=O species in the carboxylic acids with the Lewis acidic Zr sites. Interestingly, no peak was observed near 1580 $cm^{-1}$ characteristic of the formation of bidentate species. By contrast, peaks were observed at 1745, 1680 $cm^{-1}$ and ~1580 $cm^{-1}$ for 1.0ZrCp/$SiO_2$.[14,40,41] As mentioned, the first two peaks are attributable to acetic acid adsorbed on silanol groups and on Lewis-acidic Zr sites, whereas the third

peak is assigned to the formation of bidentate carboxylate species formed by the dissociative adsorption of carboxylic acids on Lewis acid pairs (see Scheme 1). Previous studies have proposed that bidentate carboxylates are the most abundant surface species formed on the surface of metal oxides during ketonization.[11–13,15,16] However, our results suggest that for isolated Zr supported on silica, monodentate carboxylate species are the active sites for ketonization of carboxylic acids. This interpretation is also in accord with recent DFT calculations over anatase $TiO_2$, which show that bidentate carboxylate species are not involved in ketonization, but act instead as spectators.[9]

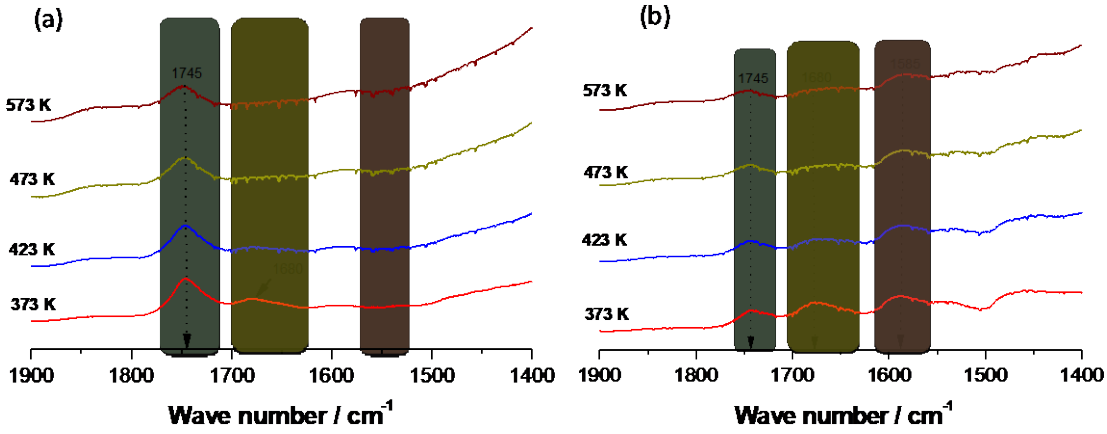


**Figure 5**. In situ FT-IR spectra of acetic acid adsorption recorded at room temperature and during desorption at various temperatures. (a) 0.1ZrCp/$SiO_2$ and (b) 1.0ZrCp/$SiO_2$ catalyst.

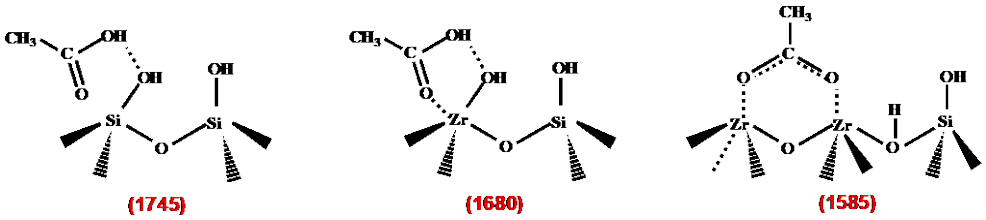


**Scheme 1.** Possible surface species formed in the ketonic decarboxylation reaction over ZrCp/$SiO_2$ catalysts and their respective FT-IR frequencies.

Additional insights into the reaction mechanism were obtained by exploring the reaction of a number of substituted carboxylic acids. Substituting the α-H of propanoic acid with one or two methyl groups decreased the rate of reaction, and carboxylic acids without any α-H were almost inactive (Figure S5). Moving the methyl group from the α- to the β-position decreased the rate of ketonization by a factor of two relative to that for carboxylic acids without any substituents. These results indicate that the presence of an α-H is crucial for ketonic decarboxylation to occur.[42]

H/D isotopic substitution was utilized to further probe the mechanism of propanoic acid ketonization over 0.1ZrCp/$SiO_2$ and 1.0ZrCp/$SiO_2$. The kinetic isotope effect, $k_H/k_D$, for ketonic decarboxylation of $CH_3COOH$ versus $CD_3COOD$ was nearly unity at 573 K (Figure S6), suggesting that abstraction of α-H is not rate limiting and that instead C-C bond formation is more critical. The conclusion that a bimolecular reaction is rate limiting for ketonization of carboxylic acids differs from previous reports that concluded that the formation of a ketene intermediate or abstraction of α-H, are rate-limiting.[43–45] Nevertheless, our findings are consistent with recent DFT calculations, which suggest that C-C bond formation to produce a β-keto acid is the kinetically relevant step in the ketonic decarboxylation of monocarboxylic acids.[12]

### 3.3 Analysis of propanoic acid ketonization

The minimum energy pathway for ketonization of propanoic acid over isolated Zr sites is shown in Scheme 2. The reaction begins with the adsorption of

two propanoic acid molecules, each one interacting with the nucleophilic oxygen of the carbonyl groups and the electrophilic Zr, as depicted in reactions 1 and 2. These elementary steps result in Zr becoming a saturated hexacoordinated species. Polarization of the carbonyl groups makes the carbon more electrophilic and the α-H more acidic, thereby facilitating abstraction of the α-H by the Lewis basic hydroxyl oxygen to form an adsorbed enolized carboxylic acid, as shown in reaction 3. As already mentioned, the formation of this enolate intermediate mirrors that of aldol condensation previously described over isolated TiOH sites.[20] Polarization of the carbonyl group encourages nucleophilic attack of the enolate on the electrophilic carbon on the second adsorbed propanoic acid molecule, leading to the formation of a C-C bond (reaction 4) in the hydroxy-β-keto acid intermediate (species E). Water leaves after the hydroxyl group on species E abstracts the proton on the Brønsted site, forming the β-keto-acid. Deprotonation of the β-keto acid and cleavage of the C-C bond leads to decarboxylation and formation of an enolized ketone. Desorption of the $CO_2$ is followed by the energetically favorable repopulation of the site with another reactant molecule to maintain Zr saturation. Subsequent proton transfer from the Brønsted site to the enol π orbital forms the final product, pentan-3-one. Desorption of the product closes the cycle, reforming intermediate B.

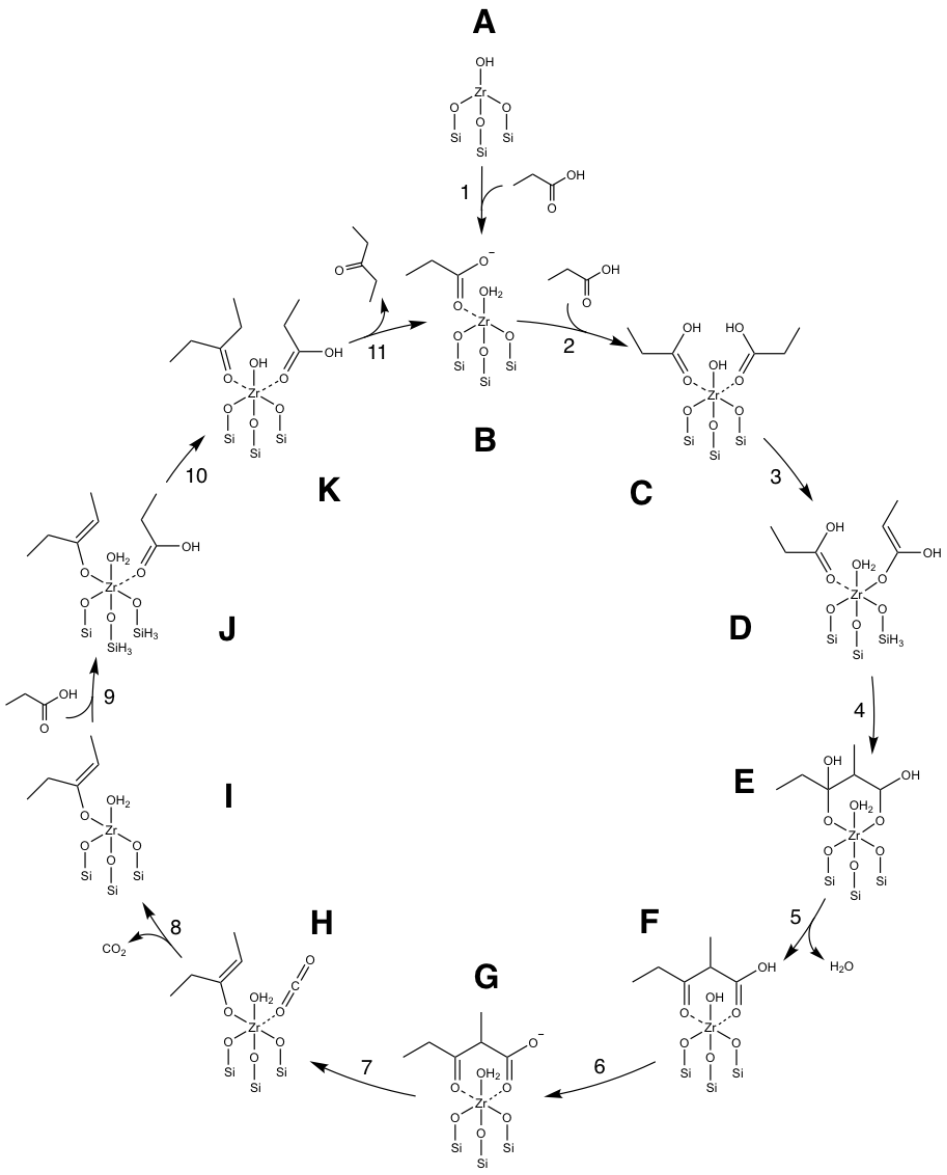


**Scheme 2.** Proposed reaction mechanism of ketonic decarboxylation of propanoic acid over isolated ZrOH to form 3-pentanone.

The predicted Gibb's free energy pathway at 573 K for the reaction sequence described in Scheme 2 is shown in Figure 6. The dissociative adsorption of propanoic acid on the empty site A forms intermediate B. The adsorption free energy for this step, reaction 1, is -2 kJ $mol^{-1}$. Because intermediate B represents the beginning of the cycle under the mechanism of Scheme 2, we designate this

state as the reference state. Our thermodynamic approximations predict adsorption of a second propanoic acid molecule to form intermediate C is approximately thermodynamically neutral at -2 kJ $mol^{-1}$. These two energetically similar states represent the lowest energy, most abundant intermediates. The largest free energy barrier corresponds to C-C bond formation (D‡) at 189 kJ $mol^{-1}$ relative to the reference state, suggesting that C-C bond formation is the rate-limiting step. This conclusion is consistent with the experimental absence of an H/D kinetic isotope effect. The overall reaction is energetically favorable, since $\Delta G_{rxn}$ = -55 kJ $mol^{-1}$.

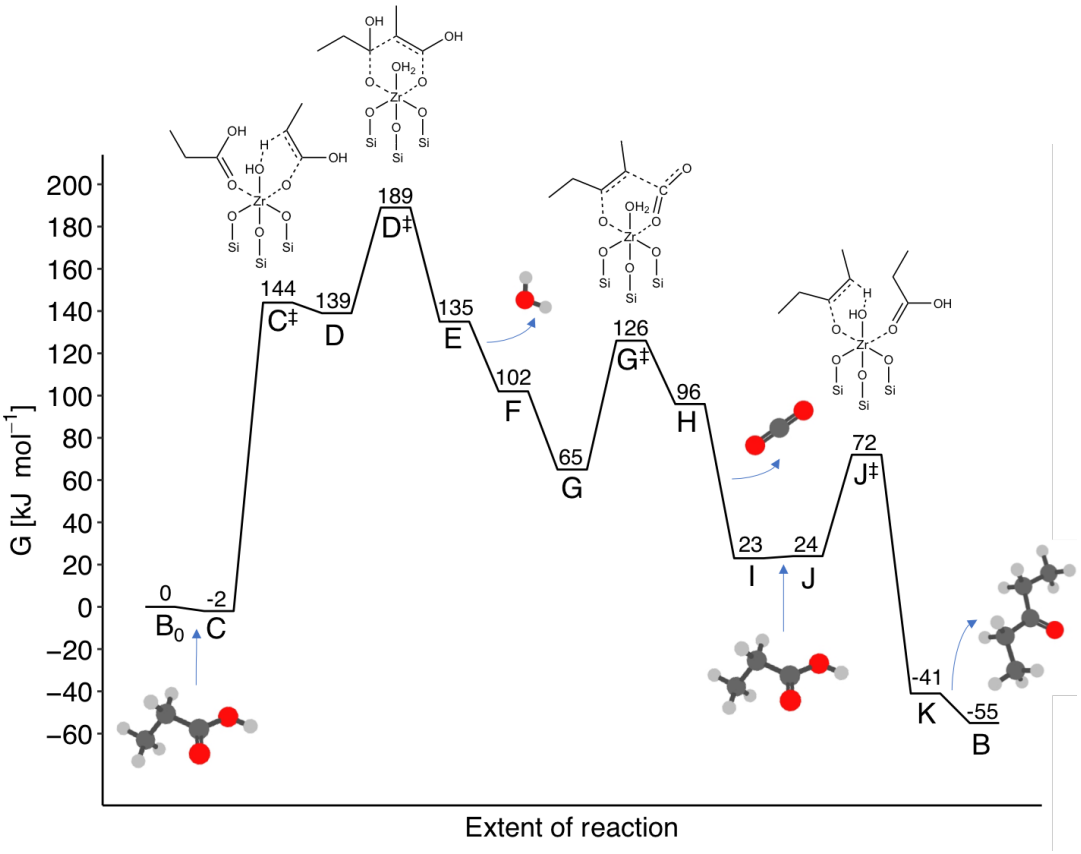


**Figure 6.** Free energy diagram for ketonic decarboxylation of propanoic acid over isolated ≡ZrOH species. The elementary steps are labeled according to the reaction sequence shown in Scheme 2. Relevant transition state structures are

depicted, as are the points where gas phase molecules enter and exit the cycle. Values were calculated at reaction conditions: T = 573 K, $P_{Total}$ = 1 atm.

A rate expression for the kinetics of propanoic acid ketonization was derived using the reaction sequence shown in Scheme 2 and the free energy profile presented in Figure 6 following the procedure described by Kozuch.[29,30] Details of this derivation are given in the Supporting Information (Equations S1-S5). Figure 7 shows the dependence of the turnover frequency (TOF) on the partial pressure of propanoic acid ($P_{acid}$) at 573 K. The model of the TOF predicts less than first order kinetics in the range of experimental reactant partial pressures (0.1 – 0.4 kPa). At higher partial pressures (greater than approximately 2 kPa), it predicts approximately zero order in $P_{acid}$.

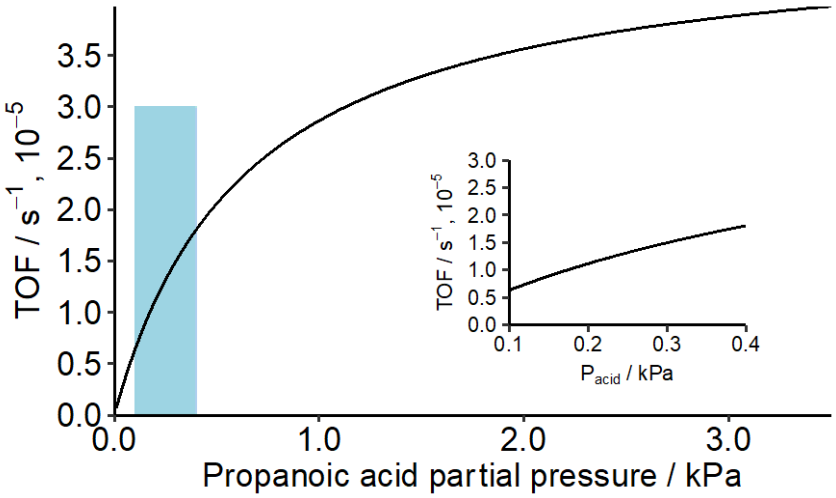


**Figure 7.** Predicted turnover frequency for ketonization of propanoic acid based on the mechanism proposed in Scheme 2 and the free energy landscape presented in Figure 6. The reaction range (0.1 – 0.4 kPa) is shaded and expanded for clarity in the inset. Reaction conditions: T = 573 K, $P_{Total}$ = 1 atm.

Under reaction conditions used in this study, the conversion of propanoic acid was < 2% and hence the concentrations of products was very small. Consequently, all terms in the rate expression that depend on product

concentration are set to zero and the TOF is well approximated by Equation 1. The percent error between this expression and the complete equation for TOF is on the order of $10^{-3}$ $s^{-1}$ for the range of $P_{acid}$ considered (Figure S7). The result is an expression for the TOF as a function of reactant partial pressure that effectively captures the character of the reaction mechanism with the free energies of states B, C, and D‡.

$$\mathrm{TOF} = \frac{k_B T}{h} \frac{P_{\mathrm{acid}}\, e^{-\Delta G_{\mathrm{rxn}}/RT}}{P_{\mathrm{acid}}\, e^{(G_{\mathrm{D}\ddagger} - G_{\mathrm{C}} - \Delta G_{\mathrm{rxn}})/RT} + e^{(G_{\mathrm{D}\ddagger} - G_{\mathrm{B}})/RT}} \quad (1)$$

The TOF is dictated by both kinetic and thermodynamic quantities. While the kinetics are determined by the transition state barrier of the rate-limiting step, $G_{\mathrm{D}\ddagger}$, the thermodynamic quantities depend on the free energy minima of the reaction (the free energies of intermediates B and C). Because $G_C - \Delta G_{\mathrm{rxn}}$ and $G_B$ are roughly equal, our model predicts the order of the TOF with respect to $P_{acid}$ is dependent on $P_{acid}$ itself and is always < 1. At vanishingly small $P_{acid}$, the second term in the denominator dominates the expression and the model predicts approximately first order kinetics. This signifies reaction equilibrium favors a singly adsorbed reactant (intermediate B) as the resting state. At high $P_{acid}$, the TOF is zero order in reactant partial pressure, signifying intermediate C is thermodynamically favored. At reaction partial pressures (0.1 – 0.4 kPa), our model predicts kinetics between zero and first order, meaning intermediates B and C are similarly favorable and contribute significantly to the overall TOF. The resting state is therefore represented by a combination of singly and doubly adsorbed reactant species.

Campbell and coworkers defined the generalized degree of rate control (DRC) as a means for quantifying the thermodynamic importance of each intermediate and the kinetic importance of each transition state for the rate of a multi-step reaction mechanism.[31,32] We performed this analysis (Equation S6-S9) in order to define the relative significance of each adsorbed species as a function of $P_{acid}$ (see Figure S8). As anticipated, we found that for the reaction conditions used in this study, both intermediates (B and C) have a significant DRC. Because both terms in the denominator of Eqn. 1 are significant, the apparent activation energy ($E_{app}$) cannot be calculated straightforwardly. This is evident on inspection of the enthalpy profile given in Figure 8. Therefore, $E_{app}$ was approximated using an expression derived by Campbell,[33] which calculates $E_{app}$ using a sum of reactive intermediate and transition state enthalpies weighted by their appropriate DRCs (Equation S4). The result is a predicted $E_{app}$ reflecting a weighted average of enthalpy differences between states $D^{\ddagger}$ and B and states $D^{\ddagger}$ and C. The predicted $E_{app}$ versus $P_{acid}$ is depicted in Figure 9.

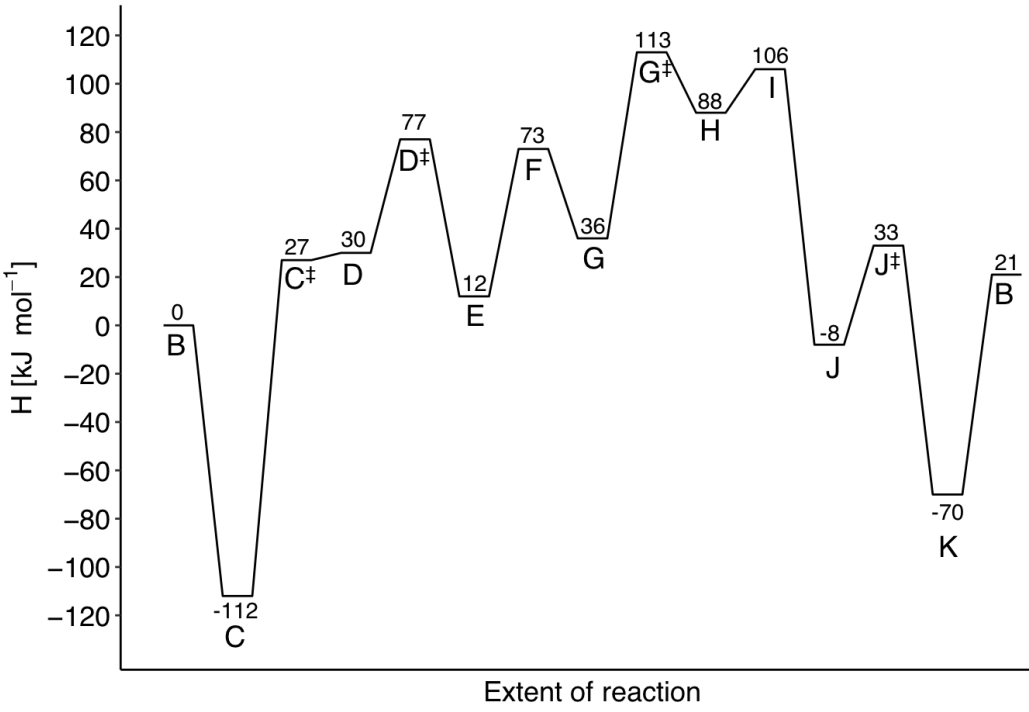


**Figure 8.** Enthalpy diagram of ketonic decarboxylation over isolated ZrOH. The elementary steps are labeled according to the reaction mechanism shown in Scheme 2. Values were calculated at reaction conditions: T = 573 K, $P_{Total}$ = 1 atm.

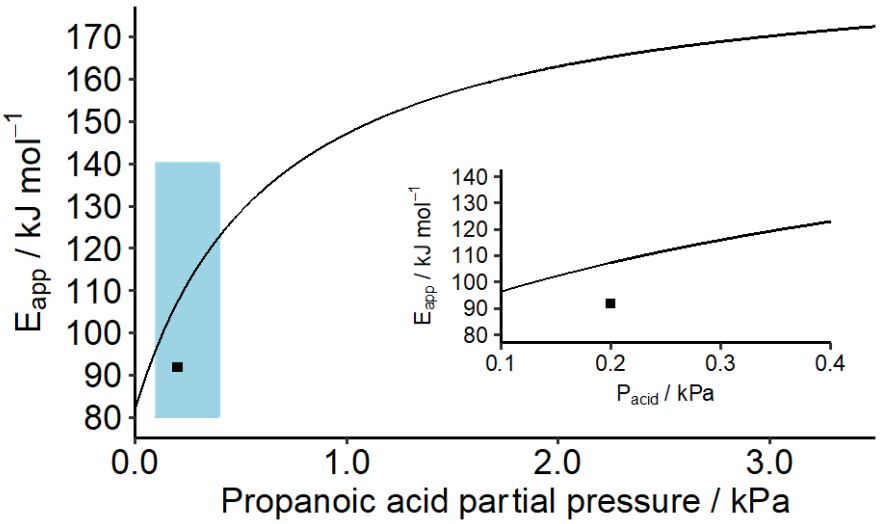


**Figure 9.** Predicted apparent activation energy of ketonic decarboxylation over isolated ZrOH as a function of reactant partial pressure. The reaction range (0.1 – 0.4 kPa) is shaded and expanded for clarity. The experimentally-observed activation barrier is depicted by a square data point. The reaction range (0.1-0.4 kPa) is shaded and expanded for clarity in the inset. Reaction conditions: T = 573 K, $P_{Total}$ = 1 atm.

Under reaction conditions (0.1-0.4 kPa), we predict $E_{app}$ to be between 96 and 124 kJ mol$^{-1}$. An Arrhenius plot of $ln(\mathrm{TOF})$ vs $1/T$ using our model of this free energy pathway under reaction conditions is in accord with this finding, predicting an $E_{app}$ of 106 kJ mol$^{-1}$ (Figure S9) at $P_{acid}$ = 0.2 kPa and T = 563-593 K. Both analyses yield values in apparent agreement with the experimentally observed $E_{app}$ of 92 kJ mol$^{-1}$. In further support of this mechanism, the predicted Gibbs activation energy of the reaction ($\Delta G^{\ddagger}$) calculated from Equation S12 is 198 kJ mol$^{-1}$, in reasonable agreement with 182 kJ mol$^{-1}$ calculated from the experimental TOF.

The model predicts a reaction order in $P_{acid}$ of 0.7, which differs from that observed experimentally, which is 0.1 between 0.1 and 0.4 kPa. We believe this discrepancy may be because our approximation of an immobile adsorbate with only quasi-harmonic vibrational modes fails to account for internal and surface rotations of adsorbed species, leading to an over-estimation of entropy loss upon adsorption ($-T\Delta S_{ads}$). This is a well-known problem of harmonic approximation techniques,[46] and implies the free energy of intermediate C is more favorable than initially predicted. We therefore conducted an analysis to examine the extent to which changes to the adsorption entropy simultaneously affect the predicted $\Delta G^{\ddagger}$, $E_{app}$, and $P_{acid}$ dependence. The results of this analysis are shown in Figure 10, which shows that relatively small changes in $-T\Delta S_{ads}$ cause significant changes in $\Delta G^{\ddagger}$, $E_{app}$, and the order in $P_{acid}$. Over the range of values of $-T\Delta S_{ads}$ shown, it is possible to achieve reasonable agreement with the values of $\Delta G^{\ddagger}$ and $E_{app}$ observed experimentally but not the order in $P_{acid}$. Alternatively, it is possible to

match the observed or in $P_{acid}$ with a 16 kJ $mol^{-1}$ adjustment to the adsorption entropy, but not the observed values of $\Delta G^{\ddagger}$ and $E_{app}$.

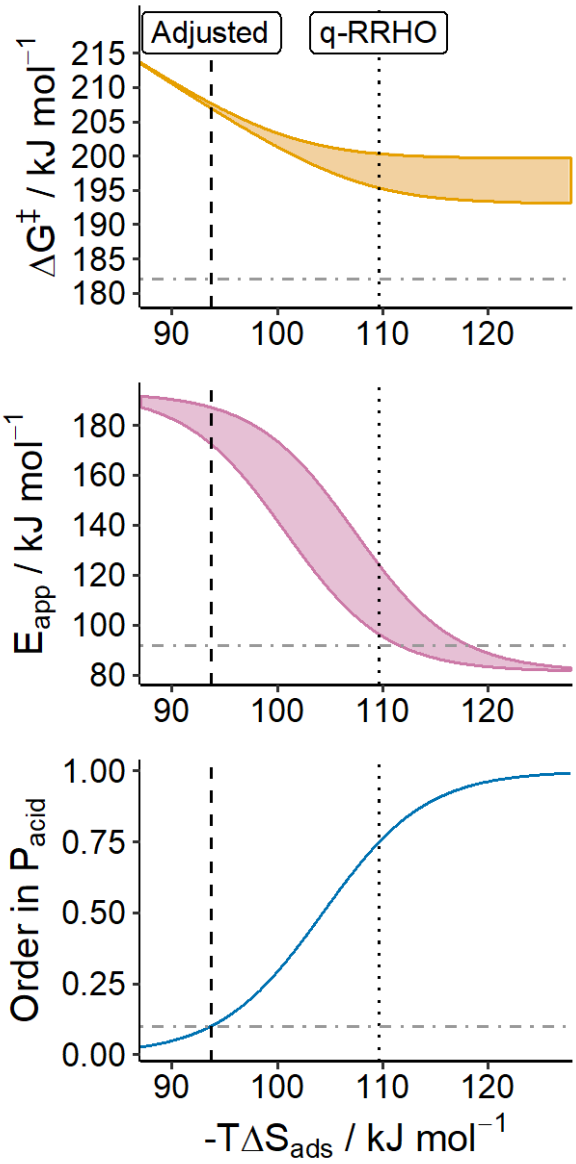


**Figure 10.** Effect of propanoic acid adsorption entropy on ketonization reaction order in partial pressure of reactant (blue, bottom), apparent activation energy (red, middle), and Gibbs activation energy (yellow, top). Each plot reflects the reaction region of $P_{acid}$ = 0.1-0.4 kPa. The vertical dotted line corresponds to the q-RRHO approximation. The horizontal dashed lines on each plot correspond to experimentally observed quantities. Reaction conditions: T = 573 K, $P_{Total}$ = 1 atm.

### 3.4 Aldol condensation of propan-2-one

To assess whether aldol condensation responds to Zr loading on $ZrCp/SiO_2$ in the same way that ketonic decarboxylation does, we also carried out a study of Zr loading on the rate of propan-2-one condensation. Experiments were conducted under conditions that ensured differential conversion (< 2%), so that catalyst deactivation and secondary aldol reactions could be minimized. The only product observed in the condensation of propan-2-one was mesityl oxide, and the rate of reaction was approximately zero order in propan-2-one partial pressure ($P_{ketone}$) in the range of 0.1 and 0.4 kPa. As seen in Figure 11, similar to the results for ketonization, a monotonic decrease in TOF occurs with increasing surface density of Zr sites (Figure 3).

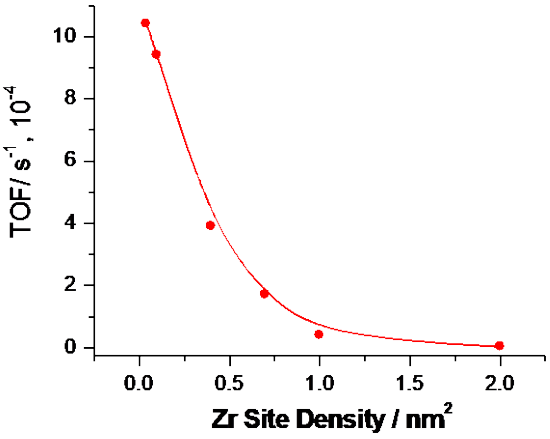


**Figure 11.** Effect of Zr site density on the activity of *x*$ZrCp/SiO_2$ for the aldol condensation of propan-2-one. Reaction conditions: T = 473 K, $P_{Total}$ = 1 atm, $Q_{Total}$ = 100 $cm^3$ $min^{-1}$, $P_{ketone} \approx 0.2$ kPa, $M_{Cat}$ = 0.1 g.

Based on previous studies of aldol condensation over TiOH sites,[20] either α-H abstraction or carbon-carbon bond formation can be the rate-limiting steps. To

establish which process is rate limiting, we measured the kinetic isotope effect for the condensation of propan-2-one. When perdeuterated propan-2-one ($(CD_3)_2CO$) was reacted over $ZrCp/SiO_2$ catalysts at 473 K, a kinetic isotope effect of unity was observed, suggesting that C-H bond cleavage is not the rate-limiting elementary step, and that C-C bond formation is rate limiting (Figure S10-11).[19] Therefore the rate-determining step involves the condensation of the enolate intermediate with another molecule of propan-2-one to form diacetone alcohol, which after dehydration produces the aldol product, mesityl oxide.

### 3.5 Analysis of propan-2-one condensation

The pathway for aldol condensation of propan-2-one over ≡ZrOH sites analyzed by DFT is shown in Scheme 3, and mirrors that proposed for aldol condensation on ≡TiOH species.[20] The associated free energy profile is given in Figure 12. The reaction begins with adsorption of the carbonyl oxygen of propan-2-one to the Lewis-acidic Zr center. Adsorption of a second propan-2-one molecule prior to enolization of the adsorbed propan-2-one causes the α-hydrogen to become more acidic, thereby facilitating abstraction of the α-proton. We note that at reaction temperature (T = 473 K), our thermal analysis predicts each adsorption to be uphill in free energy by about 11 kJ $mol^{-1}$. Following the formation of the enolate, C-C coupling of the nucleophilic carbon of the π-system to the carbonyl carbon of the non-enolized co-adsorbate forms the diacetone alcohol, with a free energy activation barrier of 114 kJ $mol^{-1}$ relative to the empty site. This is the free energy maximum of the cycle. The adsorbed diacetone alcohol readily dehydrates to form mesityl oxide.

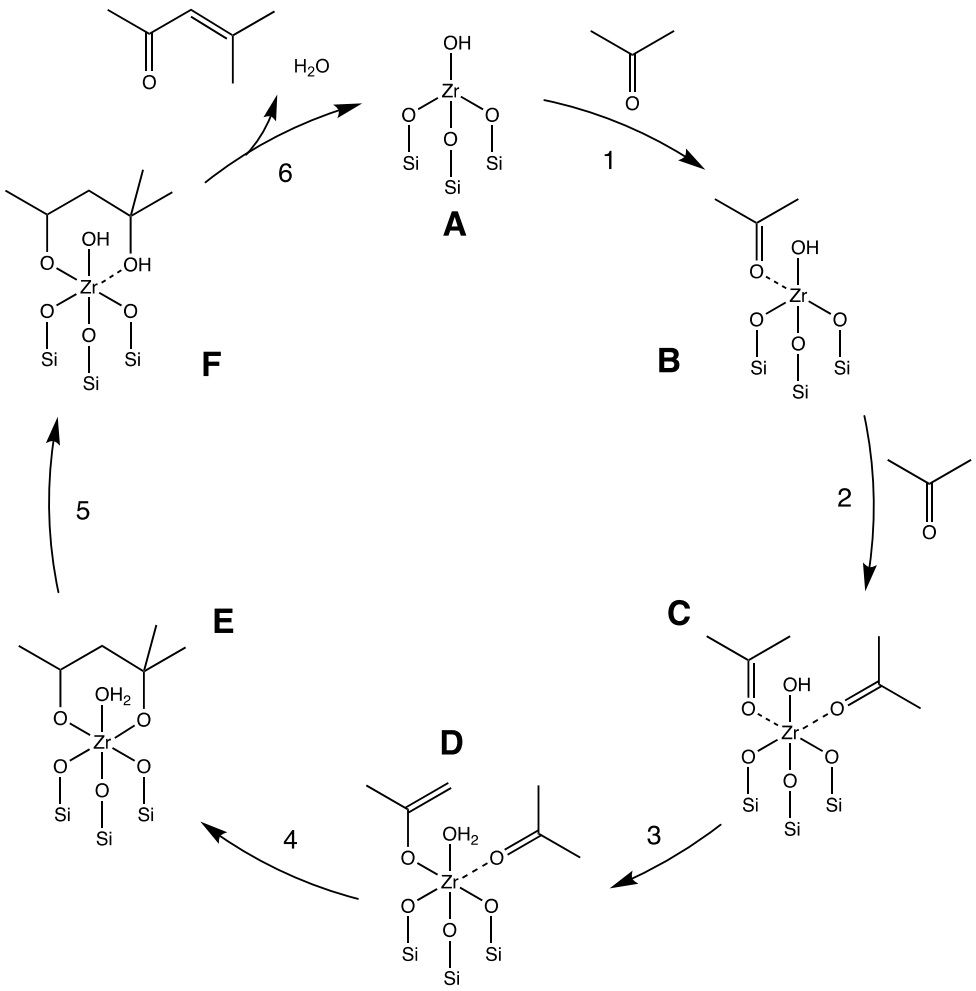


**Scheme 3.** Minimum energy reaction mechanism of aldol condensation of propan-2-one over isolated ≡ZrOH species to form mesityl oxide.

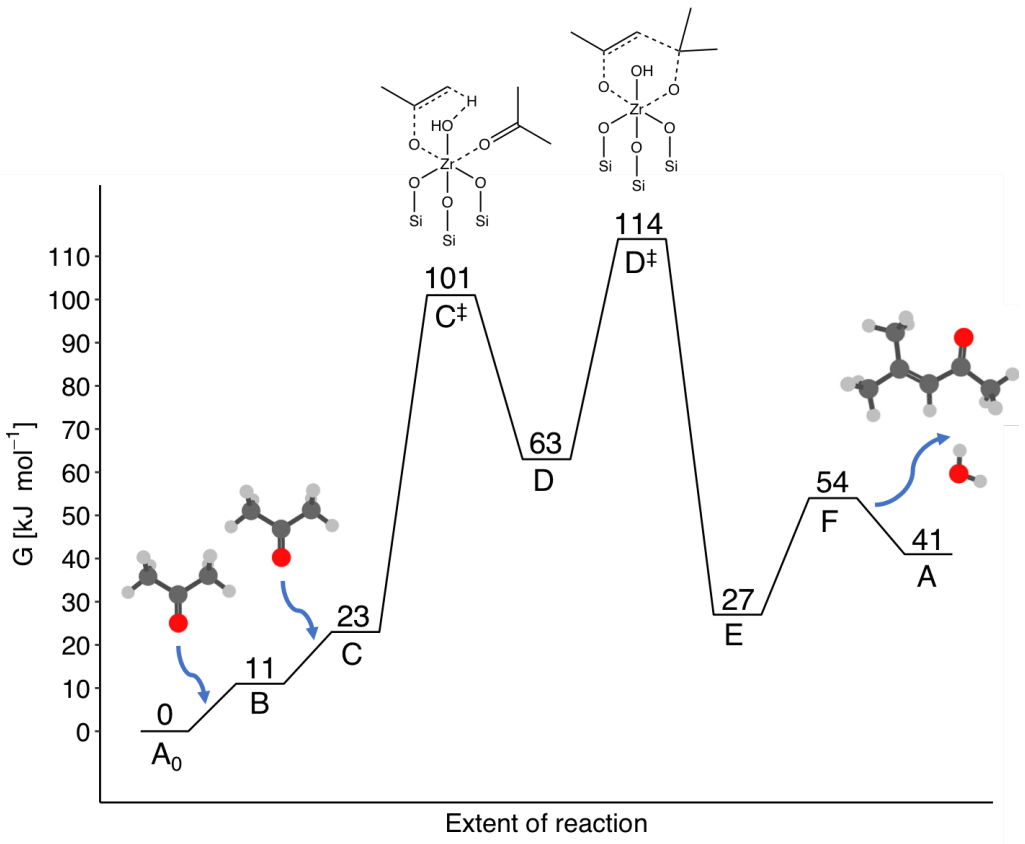


**Figure 12.** Free energy diagram for aldol condensation on isolated ≡ZrOH species. The elementary steps are labeled according to the reaction mechanism shown in Scheme 3. Relevant transition state structures are depicted alongside, as are the points where gas-phase species enter and exit the cycle. Values were calculated at reaction conditions: T = 573 K, $P_{Total}$ = 1 atm.

As with ketonization, the free energy profile suggests that the rate-limiting step is C-C bond formation (D‡), the free energy maximum in this cycle. This conclusion is consistent with an experimentally observed H/D kinetic isotope effect of unity. It is evident from the enthalpy diagram for this process (Figure 13) that the theoretically determined $E_{app}$ is strongly influenced by which adsorbed state is identified as the resting state. If either A or B is the resting state, for example, $E_{app}$ is negative, but if intermediate C is the resting state, $E_{app}$ is 70 kJ mol$^{-1}$. With the experimentally observed $E_{app}$ of 76 kJ mol$^{-1}$, intermediate C can be reasonably inferred as the resting state. The approximately zero order dependence of the

reaction rate with $P_{ketone}$ observed experimentally supports this hypothesis. However, the free energy profile predicting uphill adsorption of propan-2-one predicts a second order $P_{ketone}$ dependence. As with ketonization, we postulate our quasi-harmonic approximations to the free energy overestimate the adsorption free energy of propan-2-one to the active site.

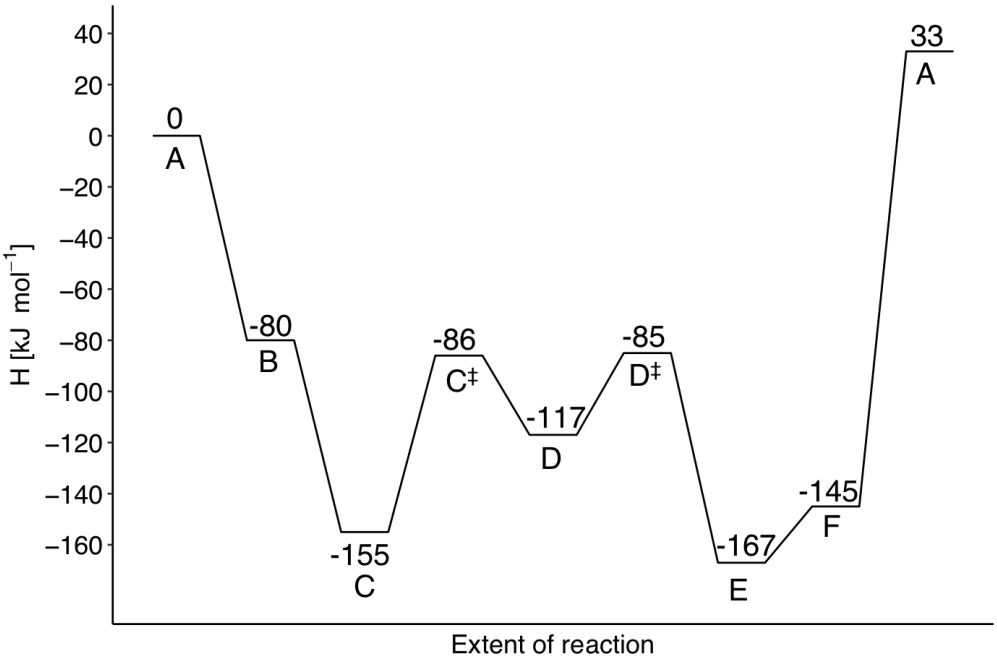


**Figure 13.** Enthalpy diagram of aldol condensation on isolated ZrOH. The elementary steps are labeled according to the reaction mechanism shown in Scheme 3. Values were calculated at reaction conditions: T = 573 K, $P_{Total}$ = 1 atm.

In light of these apparent limitations, we applied the same analysis used to investigate the effects of adjusting $-T\Delta S_{ads}$ in the ketonization reaction to aldol condensation. The computational details of the underlying TOF and degree of rate control calculations for this reaction are reported in Equations S13-S20. As depicted in Figure 14, our current free energy approximation techniques under q-

RRHO predict a reaction second order in $P_{ketone}$ with a negative $E_{app}$. Applying a -27.5 kJ $mol^{-1}$ adjustment to $-T\Delta S_{ads}$ for each propan-2-one adsorption leads to a predicted 0.1 order dependence in propan-2-one partial pressure and an $E_{app}$ in the reaction range between 57 and 70 kJ $mol^{-1}$, in good agreement with the experimentally observed $E_{app}$ of 76 kJ $mol^{-1}$. The predicted $\Delta G^{\ddagger}$, after the adjustment to $-T\Delta S_{ads}$ is applied, is between 145 and 146 kJ $mol^{-1}$ in the reaction range, in excellent agreement with 145 kJ $mol^{-1}$ calculated from experimental TOF data.

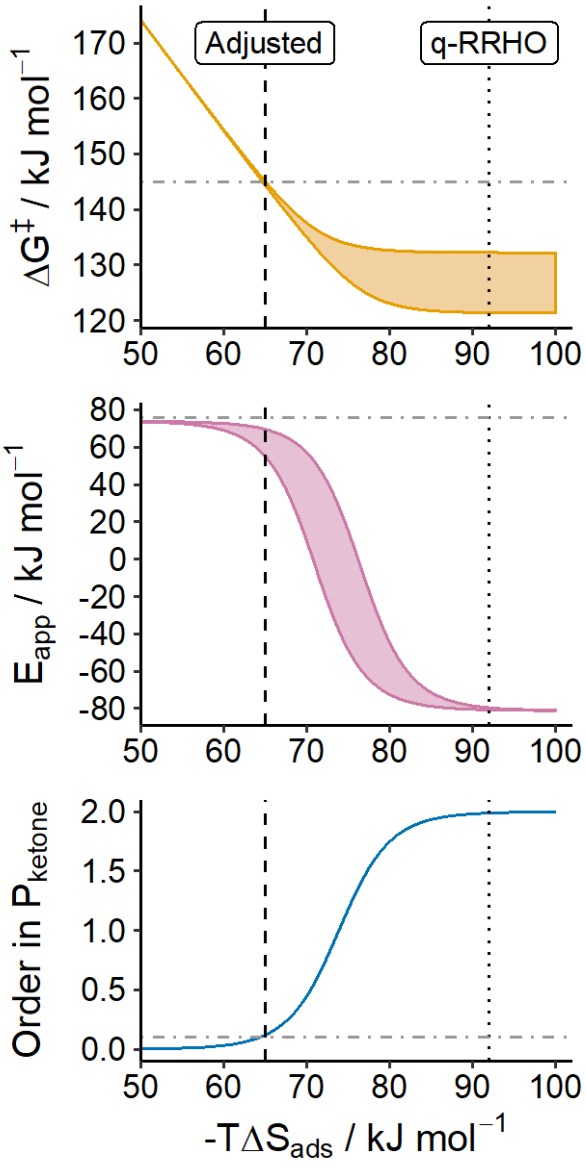


**Figure 14.** Effect of propan-2-one acid adsorption entropy on aldol condensation reaction order in partial pressure of reactant (blue, bottom), apparent activation energy (red, middle), and Gibbs activation energy (yellow, top). Each plot reflects the reaction region of $P_{ketone}$ = 0.1-0.4 kPa. The vertical dotted line corresponds to the q-RRHO approximation. The vertical dashed line reflects the required adjustment for agreement with experimental partial pressure dependence. The horizontal dashed lines on each plot correspond to experimentally observed quantities. Reaction conditions: T = 573 K, $P_{Total}$ = 1 atm.

In contrast to ketonization, the adjustment to $-T\Delta S_{ads}$ required to correct the q-RRHO approximation to 0.1 order reactant partial pressure dependence is notably larger for aldol condensation (-27.5 kJ $mol^{-1}$ for propan-2-one adsorption compared to -16 kJ $mol^{-1}$ for propanoic acid adsorption). Whereas both propan-2-one and propanoic acid are C3 oxygenates, we might expect similar error in our model of adsorption thermodynamics. We postulate this is because propanoic acid behaves more like an immobile adsorbate than propan-2-one due to the capacity of propanoic acid to hydrogen bond to the surface oxygen atoms near the adsorption site. Since propan-2-one lacks such a stabilizing force, it can retain more of its gas-phase rotational entropy upon adsorption. Indeed, factoring in the adjustment to adsorption entropy, adsorbed propan-2-one species are expected to retain approximately 17.5% of their total gas phase entropy, compared to 7% for adsorbed propanoic acid species. By comparison, rotational entropy for both propanoic acid and propan-2-one makes up about 30% of the total gas phase entropy, supporting the hypothesis that adsorbed propan-2-one may retain significantly more rotational entropy.

## 4. Conclusions

We have examined the effects of Zr coordination environment and connectivity on the rate of ketonic decarboxylation of carboxylic acids and aldol condensation of propan-2-one over silica-supported zirconia prepared by grafting Zr onto the surface of amorphous silica. The turnover frequency for both reactions decreases monotonically with increasing Zr loading, leading to the conclusion that

isolated ≡ZrOH species are more active than Zr oligomers or $ZrO_2$ nanoparticles. For both reactions, H/D isotope measurements indicate that cleavage of the α-C-H bond is not rate limiting. Instead, carbon-carbon bond formation is the rate-limiting step. Both reactions depend on the presence of a strong Lewis acid center for adsorption of either the carboxylic acid or the ketone.

Theoretical analysis of ketonic decarboxylation on isolated ≡ZrOH species suggests that the reaction mechanism for this process occurs via a β-keto acid intermediate and that isolated Zr sites remain coordinatively saturated throughout the cycle. Our analysis also suggests that C-C bond formation is the free energy maximum of the process, and is therefore the rate-limiting step. A thorough analysis of generalized degrees of rate control (DRCs) and associated partial pressure dependences suggests that both singly and doubly adsorbed propanoic acid species are significant thermodynamic intermediates under our thermodynamic approximations at reaction conditions. Varying the adsorption entropy of reactant adsorption above and below that predicted by the q-RRHO approximation, we demonstrated the sensitivity of reactant partial pressure dependence, apparent activation energy, and Gibbs activation energy to the predicted free energy of adsorption. This allowed us to quantify the degree to which our thermodynamic approximations might underestimate the entropy of adsorbed propanoic acid species, and to explain otherwise irreconcilable experimental quantities. While we found justifiable agreement between experimental and computed values among each observed value, the ensemble suggests combined limitations in computational and experimental methods.

Theoretical analysis supports the conclusion that C-C bond formation is the rate-limiting step for aldol condensation of propan-2-one. Experimental evidence suggests the resting state for this reaction is a saturated ≡ZrOH site with two adsorbed ketone molecules. Assuming that resting state, calculation of the apparent activation energy by inspection of the associated enthalpy diagram yields good agreement with experiment. The same sensitivity analysis performed for ketonization showed that we underestimate the entropy of adsorbed propan-2-one to a greater degree as adsorbed propanoic acid. Correcting for this over-approximation results in good agreement with the experimentally observed partial pressure dependence, apparent activation energy, and Gibbs activation energy.

More broadly, we have also obtained insight into the applicability of our computational methodology. Notwithstanding the pervasiveness of error in harmonic approximation techniques, the combined use of Kozuch's model of a catalytic cycle and Campbell's generalized degree of rate control allowed for both quantification of the extent of this error and the promise of reconciliation of computational studies with experimental results notwithstanding this error.

**Acknowledgements**

This work was funded by Director, Office of Science, Office of Basic Energy Sciences of the U.S. Department of Energy under Contract No. DE-AC02-05CH11231. DFT Calculations were performed on a computing cluster sponsored by the National Institutes of Health (NIH S10OD023532). We also gratefully

acknowledge the contributions of Andrew Keeton, Keyang Sun, James P. Dombrowski, and Christopher Ho to the experimental section of the manuscript.

## References

(1) Huber, G. W.; Iborra, S.; Corma, A. Synthesis of Transportation Fuels from Biomass: Chemistry, Catalysts, and Engineering. *Chem. Rev.* **2006**, *106* (9), 4044–4098. https://doi.org/10.1021/cr068360d.

(2) Chu, S.; Majumdar, A. Opportunities and Challenges for a Sustainable Energy Future. *Nature* **2012**, *488*, 294.

(3) Alonso, D. M.; Wettstein, S. G.; Dumesic, J. A. Bimetallic Catalysts for Upgrading of Biomass to Fuels and Chemicals. *Chem. Soc. Rev.* **2012**, *41* (24), 8075–8098. https://doi.org/10.1039/C2CS35188A.

(4) Climent, M. J.; Corma, A.; Iborra, S. Conversion of Biomass Platform Molecules into Fuel Additives and Liquid Hydrocarbon Fuels. *Green Chem.* **2014**, *16* (2), 516–547. https://doi.org/10.1039/C3GC41492B.

(5) Aiello-Mazzarri, C.; Agbogbo, F. K.; Holtzapple, M. T. Conversion of Municipal Solid Waste to Carboxylic Acids Using a Mixed Culture of Mesophilic Microorganisms. *Bioresour. Technol.* **2006**, *97* (1), 47–56. https://doi.org/https://doi.org/10.1016/j.biortech.2005.02.020.

(6) Corma, A.; Renz, M.; Schaverien, C. Coupling Fatty Acids by Ketonic Decarboxylation Using Solid Catalysts for the Direct Production of Diesel, Lubricants, and Chemicals. *ChemSusChem* **2008**, *1* (8-9), 739 –741. https://doi.org/10.1002/cssc.200800103.

(7) Shylesh, S.; Gokhale, A. A.; Sun, K.; Grippo, A. M.; Jadhav, D.; Yeh, A.; Ho, C. R.; Bell, A. T. Integrated Catalytic Sequences for Catalytic Upgrading of Bio-Derived Carboxylic Acids to Fuels, Lubricants and Chemical Feedstocks. *Sustain. Energy Fuels* **2017**, *1* (8), 1805–1809. https://doi.org/10.1039/C7SE00359E.

(8) Serrano-Ruiz, J. C.; Dumesic, J. A. Catalytic Routes for the Conversion of Biomass into Liquid Hydrocarbon Transportation Fuels. *Energy Environ. Sci.* **2011**, *4* (1), 83–99. https://doi.org/10.1039/C0EE00436G.

(9) Wang, S.; Iglesia, E. Experimental and Theoretical Assessment of the

Mechanism and Site Requirements for Ketonization of Carboxylic Acids on Oxides. *J. Catal.* **2017**, *345*, 183–206. https://doi.org/https://doi.org/10.1016/j.jcat.2016.11.006.

(10) Shylesh, S.; Gokhale, A. A.; Ho, C. R.; Bell, A. T. Novel Strategies for the Production of Fuels, Lubricants, and Chemicals from Biomass. *Acc. Chem. Res.* **2017**, *50* (10), 2589–2597. https://doi.org/10.1021/acs.accounts.7b00354.

(11) Pham, T. N.; Sooknoi, T.; Crossley, S. P.; Resasco, D. E. Ketonization of Carboxylic Acids: Mechanisms, Catalysts, and Implications for Biomass Conversion. *ACS Catal.* **2013**, *3* (11), 2456–2473. https://doi.org/10.1021/cs400501h.

(12) Bennett, J. A.; Parlett, C. M. A.; Isaacs, M. A.; Durndell, L. J.; Olivi, L.; Lee, A. F.; Wilson, K. Acetic Acid Ketonization over Fe3O4/SiO2 for Pyrolysis Bio-Oil Upgrading. *ChemCatChem* **2017**, *9* (9), 1648–1654. https://doi.org/10.1002/cctc.201601269.

(13) Balakrishnan, M.; Sacia, E. R.; Sreekumar, S.; Gunbas, G.; Gokhale, A. A.; Scown, C. D.; Toste, F. D.; Bell, A. T. Novel Pathways for Fuels and Lubricants from Biomass Optimized Using Life-Cycle Greenhouse Gas Assessment. *Proc. Natl. Acad. Sci.* **2015**, *112* (25), 7645 LP – 7649. https://doi.org/10.1073/pnas.1508274112.

(14) Jödicke, G.; Zenklusen, O.; Weidenhaupt, A.; Hungerbühler, K. Developing Environmentally-Sound Processes in the Chemical Industry: A Case Study on Pharmaceutical Intermediates. *J. Clean. Prod.* **1999**, *7* (2), 159–166. https://doi.org/https://doi.org/10.1016/S0959-6526(98)00075-4.

(15) Pacchioni, G. Ketonization of Carboxylic Acids in Biomass Conversion over TiO2 and ZrO2 Surfaces: A DFT Perspective. *ACS Catal.* **2014**, *4* (9), 2874–2888. https://doi.org/10.1021/cs500791w.

(16) Pulido, A.; Oliver-Tomas, B.; Renz, M.; Boronat, M.; Corma, A. Ketonic Decarboxylation Reaction Mechanism: A Combined Experimental and DFT Study. *ChemSusChem* **2013**, *6* (1), 141–151. https://doi.org/10.1002/cssc.201200419.

(17) Damyanova, S.; Grange, P.; Delmon, B. Surface Characterization of Zirconia-Coated Alumina and Silica Carriers. *J. Catal.* **1997**, *168* (2), 421–430. https://doi.org/https://doi.org/10.1006/jcat.1997.1671.

(18) Okumura, K.; Iwasawa, Y. Zirconium Oxides Dispersed on Silica Derived from $Cp_2ZrCl_2$, $[(i\text{-}PrCp)_2ZrH(\mu\text{-}H)]_2$, and $Zr(OEt)_4$Characterized by X-Ray Absorption Fine Structure and Catalytic Ketonization of Acetic Acid. *J. Catal.* **1996**, *164* (2), 440–448. https://doi.org/https://doi.org/10.1006/jcat.1996.0400.

(19) Maschmeyer, T.; Rey, F.; Sankar, G.; Thomas, J. M. Heterogeneous Catalysts Obtained by Grafting Metallocene Complexes onto Mesoporous Silica. *Nature* **1995**, *378* (6553), 159–162. https://doi.org/10.1038/378159a0.

(20) Hanna, D. G.; Shylesh, S.; Li, Y.-P.; Krishna, S.; Head-Gordon, M.; Bell, A. T. Experimental and Theoretical Study of N-Butanal Self-Condensation over Ti Species Supported on Silica. *ACS Catal.* **2014**, *4* (9), 2908–2916. https://doi.org/10.1021/cs500704b.

(21) Quadrelli, E. A.; Basset, J.-M. On Silsesquioxanes' Accuracy as Molecular Models for Silica-Grafted Complexes in Heterogeneous Catalysis. *Coord. Chem. Rev.* **2010**, *254* (5), 707–728. https://doi.org/https://doi.org/10.1016/j.ccr.2009.09.031.

(22) Chai, J.-D.; Head-Gordon, M. Systematic Optimization of Long-Range Corrected Hybrid Density Functionals. *J. Chem. Phys.* **2008**, *128* (8), 84106. https://doi.org/10.1063/1.2834918.

(23) Chai, J.-D.; Head-Gordon, M. Long-Range Corrected Hybrid Density Functionals with Damped Atom–Atom Dispersion Corrections. *Phys. Chem. Chem. Phys.* **2008**, *10* (44), 6615–6620. https://doi.org/10.1039/B810189B.

(24) Weigend, F.; Ahlrichs, R. Balanced Basis Sets of Split Valence, Triple Zeta Valence and Quadruple Zeta Valence Quality for H to Rn: Design and Assessment of Accuracy. *Phys. Chem. Chem. Phys.* **2005**, *7* (18), 3297–3305. https://doi.org/10.1039/B508541A.

(25) Weigend, F. Accurate Coulomb-Fitting Basis Sets for H to Rn. *Phys. Chem. Chem. Phys.* **2006**, *8* (9), 1057–1065. https://doi.org/10.1039/B515623H.

(26) Mallikarjun Sharada, S.; Zimmerman, P. M.; Bell, A. T.; Head-Gordon, M. Automated Transition State Searches without Evaluating the Hessian. *J. Chem. Theory Comput.* **2012**, *8* (12), 5166–5174. https://doi.org/10.1021/ct300659d.

(27) Shao, Y.; Gan, Z.; Epifanovsky, E.; Gilbert, A. T. B.; Wormit, M.; Kussmann, J.; Lange, A. W.; Behn, A.; Deng, J.; Feng, X.; et al. Advances in Molecular Quantum Chemistry Contained in the Q-Chem 4 Program Package. *Mol. Phys.* **2015**, *113* (2), 184–215. https://doi.org/10.1080/00268976.2014.952696.

(28) Grimme, S. Supramolecular Binding Thermodynamics by Dispersion-Corrected Density Functional Theory. *Chem. – A Eur. J.* **2012**, *18* (32), 9955–9964. https://doi.org/10.1002/chem.201200497.

(29) Kozuch, S.; Shaik, S. How to Conceptualize Catalytic Cycles? The Energetic Span Model. *Acc. Chem. Res.* **2011**, *44* (2), 101–110. https://doi.org/10.1021/ar1000956.

(30) Kozuch, S. A Refinement of Everyday Thinking : The Energetic Span Model for Kinetic Assessment of Catalytic Cycles. *WIREs Comput Mol Sci* **2012**, *2*, 795–815. https://doi.org/10.1002/wcms.1100.

(31) Campbell, C. T. The Degree of Rate Control: A Powerful Tool for Catalysis Research. *ACS Catal.* **2017**, *7* (4), 2770–2779. https://doi.org/10.1021/acscatal.7b00115.

(32) Stegelmann, C.; Andreasen, A.; Campbell, C. T. Degree of Rate Control: How Much the Energies of Intermediates and Transition States Control Rates. *J. Am. Chem. Soc.* **2009**, *131* (23), 8077–8082. https://doi.org/10.1021/ja9000097.

(33) Mao, Z.; Campbell, C. T. Apparent Activation Energies in Complex Reaction Mechanisms: A Simple Relationship via Degrees of Rate Control. *ACS Catal.* **2019**, 9465–9473. https://doi.org/10.1021/acscatal.9b02761.

(34) Li, M.; Feng, Z.; Xiong, G.; Ying, P.; Xin, Q.; Li, C. Phase Transformation in the Surface Region of Zirconia Detected by UV Raman Spectroscopy. *J. Phys. Chem. B* **2001**, *105* (34), 8107–8111. https://doi.org/10.1021/jp010526l.

(35) Jensen, M. B.; Morandi, S.; Prinetto, F.; Sjåstad, A. O.; Olsbye, U.; Ghiotti, G. FT-IR Characterization of Supported Ni-Catalysts: Influence of Different Supports on the Metal Phase Properties. *Catal. Today* **2012**, *197* (1), 38–49. https://doi.org/https://doi.org/10.1016/j.cattod.2012.06.016.

(36) Lavalley, J. C. Infrared Spectrometric Studies of the Surface Basicity of Metal Oxides and Zeolites Using Adsorbed Probe Molecules. *Catal. Today* **1996**, *27* (3), 377–401. https://doi.org/https://doi.org/10.1016/0920-5861(95)00161-1.

(37) Shylesh, S.; Hanna, D.; Werner, S.; Bell, A. T. Factors Influencing the Activity, Selectivity, and Stability of Rh-Based Supported Ionic Liquid Phase (SILP) Catalysts for Hydroformylation of Propene. *ACS Catal.* **2012**, *2* (4), 487–493. https://doi.org/10.1021/cs2004888.

(38) Bouh, A. O.; Rice, G. L.; Scott, S. L. Mono- and Dinuclear Silica-Supported Titanium(IV) Complexes and the Effect of TiOTi Connectivity on Reactivity. *J. Am. Chem. Soc.* **1999**, *121* (31), 7201–7210. https://doi.org/10.1021/ja9829160.

(39) Shylesh, S.; Kim, D.; Gokhale, A. A.; Canlas, C. G.; Struppe, J. O.; Ho, C. R.; Jadhav, D.; Yeh, A.; Bell, A. T. Effects of Composition and Structure of

Mg/Al Oxides on Their Activity and Selectivity for the Condensation of Methyl Ketones. *Ind. Eng. Chem. Res.* **2016**, *55* (40), 10635–10644. https://doi.org/10.1021/acs.iecr.6b03601.

(40) Panchenko, V. N.; Zaytseva, Y. A.; Simonov, M. N.; Simakova, I. L.; Paukshtis, E. A. DRIFTS and UV–Vis DRS Study of Valeric Acid Ketonization Mechanism over ZrO2 in Hydrogen Atmosphere. *J. Mol. Catal. A Chem.* **2014**, *388–389*, 133–140. https://doi.org/https://doi.org/10.1016/j.molcata.2013.11.012.

(41) Pei, Z.-F.; Ponec, V. On the Intermediates of the Acetic Acid Reactions on Oxides: An IR Study. *Appl. Surf. Sci.* **1996**, *103* (2), 171–182. https://doi.org/https://doi.org/10.1016/0169-4332(96)00453-9.

(42) Nagashima, O.; Sato, S.; Takahashi, R.; Sodesawa, T. Ketonization of Carboxylic Acids over CeO2-Based Composite Oxides. *J. Mol. Catal. A Chem.* **2005**, *227* (1), 231–239. https://doi.org/https://doi.org/10.1016/j.molcata.2004.10.042.

(43) Randery, S. D.; Warren, J. S.; Dooley, K. M. Cerium Oxide-Based Catalysts for Production of Ketones by Acid Condensation. *Appl. Catal. A Gen.* **2002**, *226* (1), 265–280. https://doi.org/https://doi.org/10.1016/S0926-860X(01)00912-7.

(44) Dooley, K. M.; Bhat, A. K.; Plaisance, C. P.; Roy, A. D. Ketones from Acid Condensation Using Supported CeO2 Catalysts: Effect of Additives. *Appl. Catal. A Gen.* **2007**, *320*, 122–133. https://doi.org/https://doi.org/10.1016/j.apcata.2007.01.021.

(45) Hendren, T. S.; Dooley, K. M. Kinetics of Catalyzed Acid/Acid and Acid/Aldehyde Condensation Reactions to Non-Symmetric Ketones. *Catal. Today* **2003**, *85* (2), 333–351. https://doi.org/https://doi.org/10.1016/S0920-5861(03)00399-7.

(46) Campbell, C. T.; Sellers, J. R. V. The Entropies of Adsorbed Molecules. *J. Am. Chem. Soc.* **2012**, *134* (43), 18109–18115. https://doi.org/10.1021/ja3080117.

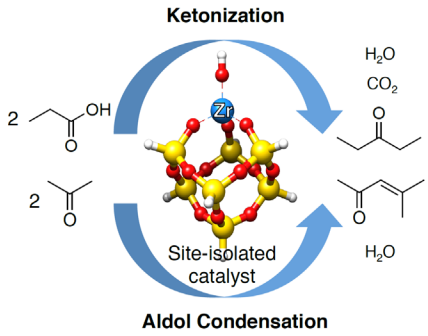


**Table of Contents Graphic**

# Supporting Information

# Experimental and Computational Studies of Carbon-Carbon Bond Formation via Ketonization and Aldol Condensation over Site-Isolated Zirconium Catalysts

Sankaranarayanapillai Shylesh,[‡,a] Lance A. Bettinson, [‡,a,b], Ahmed Aljahri,[a] Martin Head-Gordon,[a,c] and Alexis T. Bell*[a,b]

[a]Chemical Sciences Division, Lawrence Berkeley National Laboratory, Berkeley, CA 94720

[b]Department of Chemical and Biomolecular Engineering, University of California, Berkeley, California 94720

[c]Department of Chemistry, University of California, Berkeley, California 94720

Submitted to
ACS Catalysis

[‡]Contributed to the work equally
*To whom correspondence should be addressed

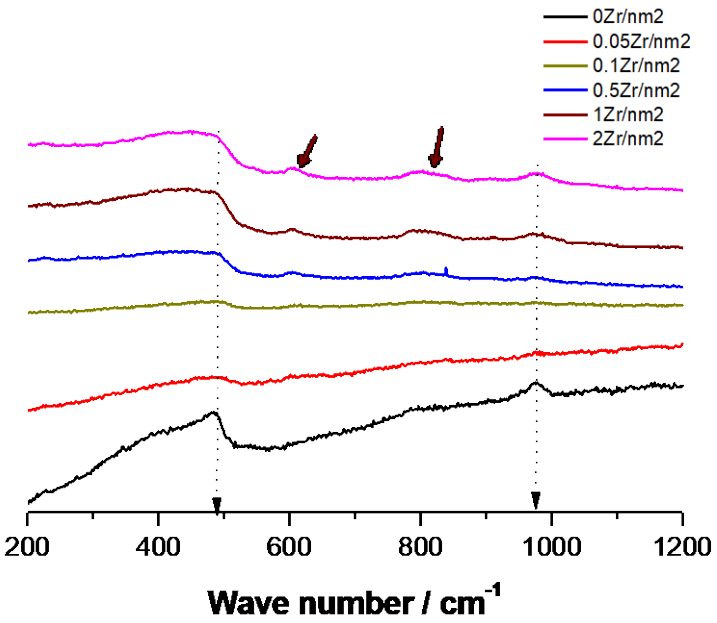


**Figure S1**. Raman spectra of support silica and various Zr loaded silica samples.

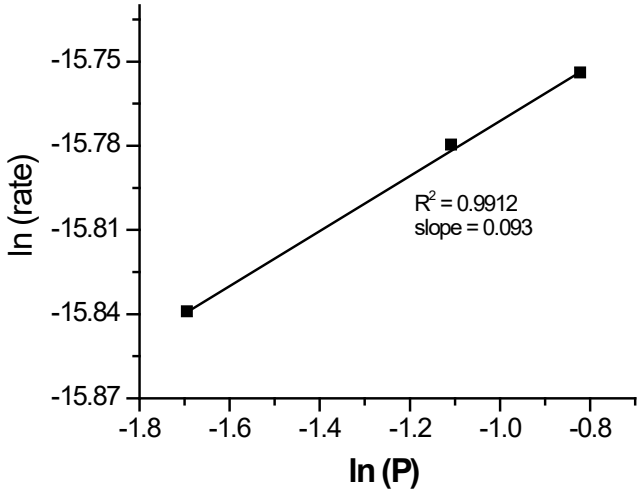


**Figure S2**. Partial pressure dependency of 0.1ZrCp/SiO2 catalysts in the ketonization reaction of propanoic acid.

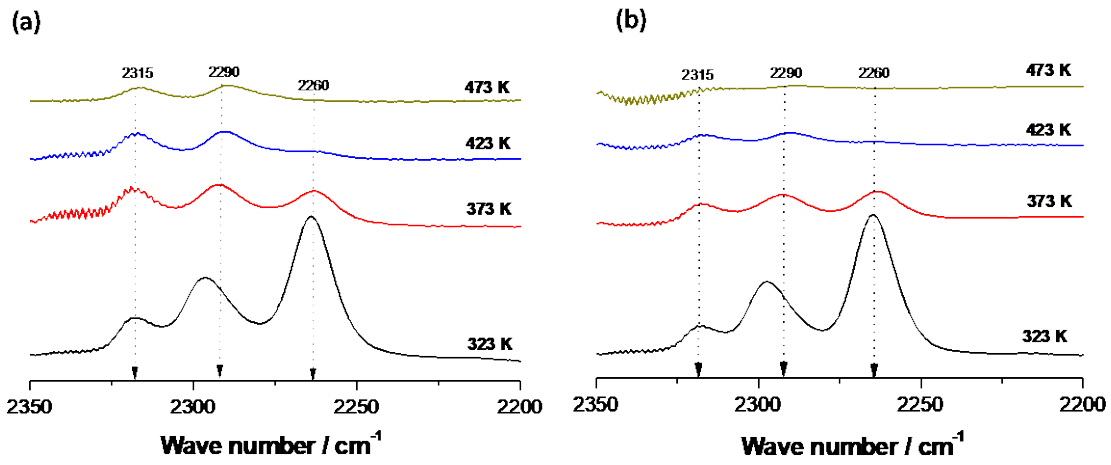


**Figure S3**. In situ FT-IR spectra of $CH_3CN$ adsorption at room temperature and its desorption at various temperatures. (a) $0.1ZrCp/SiO_2$ and (b) $1.0ZrCp/SiO_2$ catalyst.

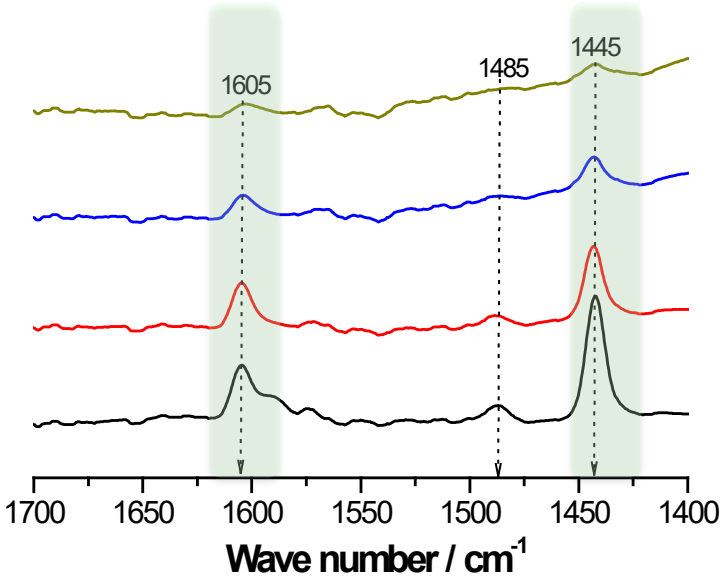


**Figure S4**. Pyridine IR studies over a $ZrCp/SiO_2$ catalyst. Lewis acid sites are noted in the IR spectrum and a decrease in peak intensity is noted with an increase in temperature from 50 °C to 200 °C (bottom to top).

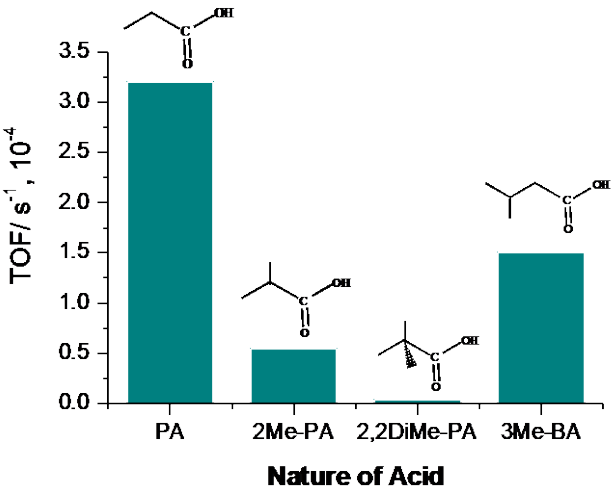


**Figure S5**. Catalytic activity of propanoic acid and various substituted carboxylic acids in the ketonization reactions, where PA = propanoic acid, 2Me-PA = 2-methyl propanoic acid, 2,2DiMe-PA=2,2 dimethyl propanoic aid and 3Me-BA=3-methyl butric acid. Reaction conditions: T = 573 K, $P_{Total}$ = 1 atm, $Q_{Total}$ = 100 $cm^3$ $min^{-1}$, $P_{reactant}$ ≈ 0.2 kPa, $M_{Cat}$ = 0.1 g.

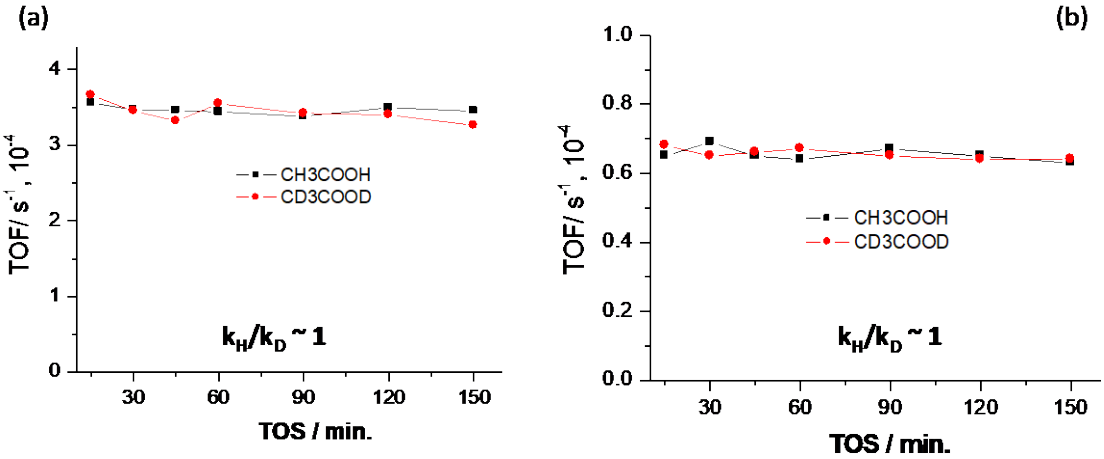


**Figure S6**. Kinetic isotope effect over (a) 0.1ZrCp/$SiO_2$ and (b) 1.0ZrCp/$SiO_2$ catalyst using acetic acid and deuterated acetic acid substrate. Reaction conditions: T = 573 K, $P_{Total}$ = 1 atm, $Q_{Total}$ = 100 $cm^3$ $min^{-1}$, $P_{acid}$ ≈ 0.2 kPa, $M_{Cat}$ = 0.1 g.

## Energetic span model considering reactant and product partial pressures

We model the turnover frequency using the energetic span model derived by Kozuch, which considers all intermediate states, transition states, and effects of reactant and product partial pressures:[26,27]

$$\mathrm{TOF} = \frac{k_B T}{h} \frac{e^{-\Delta G_{\mathrm{rxn}}/RT} \prod_h [R_h] - \prod_h [P_h]}{\sum_{ij} e^{\left(T_i - I_j - \delta G'_{ij}\right)/RT} \prod_h \delta R'_{h,ij}\, \delta P_{h,ij}} \tag{S1}$$

$$= \frac{k_B T}{h} \frac{e^{-\Delta G_{\mathrm{rxn}}/RT} P_{\mathrm{acid}}^2 - P_{H_2O} P_{CO_2} P_{\mathrm{ketone}}}{\sum_{i,j=1}^{10} e^{\left(T_i - I_j - \delta G'_{ij}\right)/RT} \prod_h \delta R'_{h,ij}\, \delta P_{h,ij}} \tag{S2}$$

$$\delta G'_{ij} = \begin{cases} \Delta G_{\mathrm{rxn}} & \text{if } i > j \\ 0 & \text{if } i \leq j \end{cases}$$

Here, $T_i$ refers to the free energy of the $i^{th}$ transition state before the $i^{th}$ intermediate, and $I_j$ refers to the free energy of the $j^{th}$ intermediate state after the $j^{th}$ transition state. All values of $T_i$ and $I_j$ are energies with respect to a single reference state. Where there is no explicit transition state for $T_i$, the transition state is considered to be the higher of the previous intermediate $I_{i-1}$ and the following intermediate $I_i$.

The term $\delta R'_{ij}$ is equal to the partial pressure of reactant $h$ if, between intermediate $I_j$ and $T_i$, the reactant is *not* consumed, and is equal to unity otherwise. The term $\delta P_{ij}$, on the other hand, is equal to the partial pressure of product $h$ if, between intermediate $I_j$ and $T_i$, the reactant is consumed, and is equal to unity otherwise. Reactants that enter the catalytic cycle are considered to do so on the uphill of the relevant transition state's formation, while products that leave the catalytic cycle are considered to do so on the downhill from the relevant transition state. The result for the partial pressure term in the denominator for all $i$ and $j$ in this reaction is:

$$\prod_h \delta R'_{h,ij}\, \delta P_{h,ij} =$$

$$\begin{bmatrix}
P_{H_2O}P_{CO_2}P_{\mathrm{ketone}} & P_{H_2O}P_{CO_2}P_{\mathrm{ketone}} & P_{H_2O}P_{CO_2}P_{\mathrm{ketone}} & P_{CO_2}P_{\mathrm{ketone}} & P_{CO_2}P_{\mathrm{ketone}} & P_{CO_2}P_{\mathrm{ketone}} & P_{\mathrm{ketone}} & P_{\mathrm{acid}}P_{\mathrm{ketone}} & P_{\mathrm{acid}}P_{\mathrm{ketone}} & P_{\mathrm{acid}} \\
P_{\mathrm{acid}}^2 & P_{H_2O}P_{CO_2}P_{\mathrm{ketone}} & P_{H_2O}P_{CO_2}P_{\mathrm{ketone}} & P_{CO_2}P_{\mathrm{ketone}} & P_{CO_2}P_{\mathrm{ketone}} & P_{CO_2}P_{\mathrm{ketone}} & P_{\mathrm{ketone}} & P_{\mathrm{acid}}P_{\mathrm{ketone}} & P_{\mathrm{acid}}P_{\mathrm{ketone}} & P_{\mathrm{acid}} \\
P_{\mathrm{acid}}^2 & P_{\mathrm{acid}}^2 & P_{H_2O}P_{CO_2}P_{\mathrm{ketone}} & P_{CO_2}P_{\mathrm{ketone}} & P_{CO_2}P_{\mathrm{ketone}} & P_{CO_2}P_{\mathrm{ketone}} & P_{\mathrm{ketone}} & P_{\mathrm{acid}}P_{\mathrm{ketone}} & P_{\mathrm{acid}}P_{\mathrm{ketone}} & P_{\mathrm{acid}} \\
P_{\mathrm{acid}}^2 & P_{\mathrm{acid}}^2 & P_{\mathrm{acid}}^2 & P_{CO_2}P_{\mathrm{ketone}} & P_{CO_2}P_{\mathrm{ketone}} & P_{CO_2}P_{\mathrm{ketone}} & P_{\mathrm{ketone}} & P_{\mathrm{acid}}P_{\mathrm{ketone}} & P_{\mathrm{acid}}P_{\mathrm{ketone}} & P_{\mathrm{acid}} \\
P_{\mathrm{acid}}^2P_{H_2O} & P_{\mathrm{acid}}^2P_{H_2O} & P_{\mathrm{acid}}^2P_{H_2O} & P_{\mathrm{acid}}^2 & P_{H_2O}P_{CO_2}P_{\mathrm{ketone}} & P_{H_2O}P_{CO_2}P_{\mathrm{ketone}} & P_{H_2O}P_{CO_2}P_{\mathrm{ketone}} & P_{H_2O}P_{CO_2}P_{\mathrm{ketone}} & P_{\mathrm{acid}}P_{H_2O}P_{\mathrm{ketone}} & P_{\mathrm{acid}}P_{H_2O}P_{\mathrm{ketone}} & P_{\mathrm{acid}}P_{H_2O} \\
P_{\mathrm{acid}}^2P_{H_2O} & P_{\mathrm{acid}}^2P_{H_2O} & P_{\mathrm{acid}}^2P_{H_2O} & P_{\mathrm{acid}}^2 & P_{\mathrm{acid}}^2 & P_{H_2O}P_{CO_2}P_{\mathrm{ketone}} & P_{H_2O}P_{CO_2}P_{\mathrm{ketone}} & P_{H_2O}P_{CO_2}P_{\mathrm{ketone}} & P_{\mathrm{acid}}P_{H_2O}P_{\mathrm{ketone}} & P_{\mathrm{acid}}P_{H_2O}P_{\mathrm{ketone}} & P_{\mathrm{acid}}P_{H_2O} \\
P_{\mathrm{acid}}^2P_{H_2O} & P_{\mathrm{acid}}^2P_{H_2O} & P_{\mathrm{acid}}^2P_{H_2O} & P_{\mathrm{acid}}^2 & P_{\mathrm{acid}}^2 & P_{\mathrm{acid}}^2 & P_{H_2O}P_{CO_2}P_{\mathrm{ketone}} & P_{\mathrm{acid}}P_{H_2O}P_{\mathrm{ketone}} & P_{\mathrm{acid}}P_{H_2O}P_{\mathrm{ketone}} & P_{\mathrm{acid}}P_{H_2O} \\
P_{\mathrm{acid}}P_{H_2O}P_{CO_2} & P_{\mathrm{acid}}P_{H_2O}P_{CO_2} & P_{\mathrm{acid}}P_{H_2O}P_{CO_2} & P_{\mathrm{acid}}P_{CO_2} & P_{\mathrm{acid}}P_{CO_2} & P_{\mathrm{acid}}P_{CO_2} & P_{\mathrm{acid}} & P_{H_2O}P_{CO_2}P_{\mathrm{ketone}} & P_{H_2O}P_{CO_2}P_{\mathrm{ketone}} & P_{H_2O}P_{CO_2} \\
P_{\mathrm{acid}}P_{H_2O}P_{CO_2} & P_{\mathrm{acid}}P_{H_2O}P_{CO_2} & P_{\mathrm{acid}}P_{H_2O}P_{CO_2} & P_{\mathrm{acid}}P_{CO_2} & P_{\mathrm{acid}}P_{CO_2} & P_{\mathrm{acid}}P_{CO_2} & P_{\mathrm{acid}} & P_{\mathrm{acid}}^2 & P_{H_2O}P_{CO_2}P_{\mathrm{ketone}} & P_{H_2O}P_{CO_2} \\
P_{\mathrm{acid}}P_{H_2O}P_{CO_2} & P_{\mathrm{acid}}P_{H_2O}P_{CO_2} & P_{\mathrm{acid}}P_{H_2O}P_{CO_2} & P_{\mathrm{acid}}P_{CO_2} & P_{\mathrm{acid}}P_{CO_2} & P_{\mathrm{acid}}P_{CO_2} & P_{\mathrm{acid}} & P_{\mathrm{acid}}^2 & P_{\mathrm{acid}}^2 & P_{H_2O}P_{CO_2}
\end{bmatrix} \tag{S3}$$

Equation S3 simplifies when product partial pressures ($P_{H_2O}$, $P_{CO_2}$, and $P_{\mathrm{ketone}}$) are approximated as zero. This assumption is deemed appropriate because the reaction is considered under differential conditions, meaning the

conversion of products to reactants is less than 2%. Therefore, only a few terms in the matrix need to be considered:

$$\prod_h \delta R'_{h,ij}\,\delta P_{h,ij} = \begin{bmatrix} 0 & \cdots & \cdots & \cdots & \cdots & \cdots & \cdots & \cdots & 0 & P_{\text{acid}} \\ P_{\text{acid}}^2 & \ddots & & & & & & & \vdots & P_{\text{acid}} \\ P_{\text{acid}}^2 & P_{\text{acid}}^2 & \ddots & & & & & & \vdots & P_{\text{acid}} \\ P_{\text{acid}}^2 & P_{\text{acid}}^2 & P_{\text{acid}}^2 & 0 & & & & & \vdots & P_{\text{acid}} \\ 0 & \cdots & 0 & P_{\text{acid}}^2 & \ddots & & & & \vdots & 0 \\ \vdots & \ddots & \vdots & P_{\text{acid}}^2 & P_{\text{acid}}^2 & \ddots & & & \vdots & \vdots \\ \vdots & & \vdots & P_{\text{acid}}^2 & P_{\text{acid}}^2 & P_{\text{acid}}^2 & 0 & & \vdots & \vdots \\ \vdots & & 0 & \cdots & \cdots & 0 & P_{\text{acid}} & \ddots & \vdots & \vdots \\ \vdots & & & & & \vdots & P_{\text{acid}} & P_{\text{acid}}^2 & \ddots & \vdots \\ 0 & \cdots & \cdots & \cdots & \cdots & 0 & P_{\text{acid}} & P_{\text{acid}}^2 & P_{\text{acid}}^2 & 0 \end{bmatrix} \quad \text{(S4)}$$

The exponential terms in the denominator of Equation S2 are dominated by the combinations of transition state ($T_i$) and intermediate ($I_j$) free energies whose differences are greatest. Therefore, the TOF can be further simplified considering only the dominant combinations of $T_i$ and $I_j$. In our case, the free energy difference of the C-C bond formation transition state (D‡) and the singly adsorbed propanoic acid state B ($T_3 - I_{10/0}$), and the difference in free energy of D‡ and the doubly adsorbed propanoic acid state C ($T_3 - I_1$) are sufficiently large that their exponential values overwhelmingly dominate the denominator of Equation S2. Their associated partial pressure weights are indicated in red text in Equation S4. The TOF simplifies to

$$\text{TOF} = \frac{k_B T}{h} \frac{e^{-\Delta G_{\text{rxn}}/RT} P_{\text{acid}}^2}{P_{\text{acid}}^2 e^{T_3 - I_1 - \Delta G_{\text{rxn}}} + P_{\text{acid}} e^{T_3 - I_{10}}} \quad \text{(S5)}$$

Equation S5 is identical to Equation 1 in the main text. The percent error of this simplification to the full implementation of the model is given in Figure S7, and is on the order of $10^{-3}$ % for all relevant values of reactant partial pressure.

**Generalized degrees of rate control and apparent activation energy**

Using our expression of TOF derived from the energetic span model, we quantified the relative importance of each intermediate and transition state (denoted by the index $i$) to the total rate using an expression derived by Campbell.[28]

$$X_i = \frac{\partial(\ln \mathrm{TOF})}{\partial\left(\frac{-G_i}{RT}\right)} \qquad \text{(S6)}$$

Since our TOF expression depends on the energies of three intermediates and transition states, DRCs for these intermediates were calculated using Equation S1.

$$X_B = -\frac{e^{(G_C+\Delta G_{\mathrm{rxn}})/RT}}{P_{\mathrm{acid}}e^{G_B/RT} + e^{(G_C+\Delta G_{\mathrm{rxn}})/RT}} \qquad \text{(S7)}$$

$$X_C = -\frac{P_{\mathrm{acid}}e^{G_B/RT}}{P_{\mathrm{acid}}e^{G_B/RT} + e^{(G_C+\Delta G_{\mathrm{rxn}})/RT}} \qquad \text{(S8)}$$

$$X_{D^\ddagger} = 1 \qquad \text{(S9)}$$

The dependence of the intermediate DRCs on reactant partial pressure is shown in Figure S7. The apparent activation energy is then calculated as a sum of RT and each intermediate and transition state enthalpy, weighted by their respective DRCs.[30] The result is an apparent activation energy as a function of reactant partial pressure.

$$E_{app} = RT + X_B H_B^0 + X_C H_C^0 + X_{D^\ddagger} H_{D^\ddagger}^0 \qquad \text{(S10)}$$

**Gibbs activation energy**

As with the derivation for Kozuch's energetic span model, the effective rate of the reaction can be related to an effective Gibbs free energy of activation for the reaction.

$$\mathrm{TOF} = \frac{k_B T}{h} e^{\Delta G^\ddagger/RT} \qquad \text{(S11)}$$

$$\Delta G^\ddagger = RT \ln\left(\frac{h}{k_B T} \times \mathrm{TOF}\ \right) \qquad \text{(S12)}$$

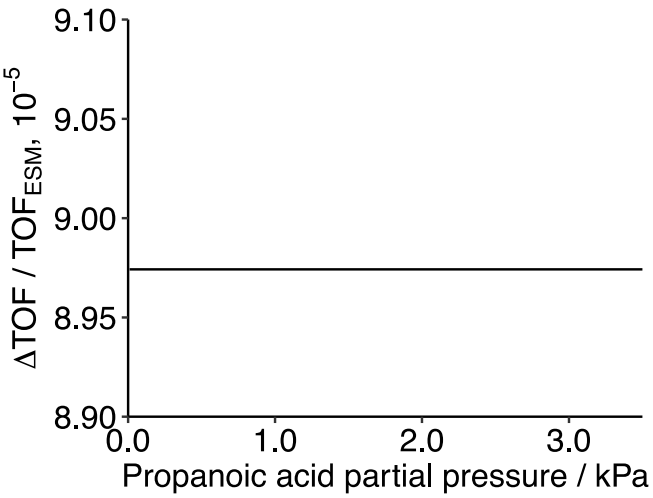


**Figure S7.** Error between Equation 1 and the energetic span model. ΔTOF = $TOF_{Eqn\ 1} - TOF_{ESM}$.

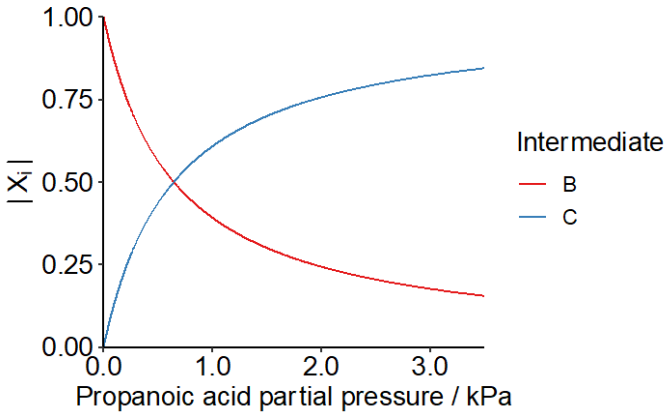


**Figure S8**. Relative degrees of TOF control of ketonization intermediates B and C as a function of reactant partial pressure, based on the approximation of TOF given in Equation 1.

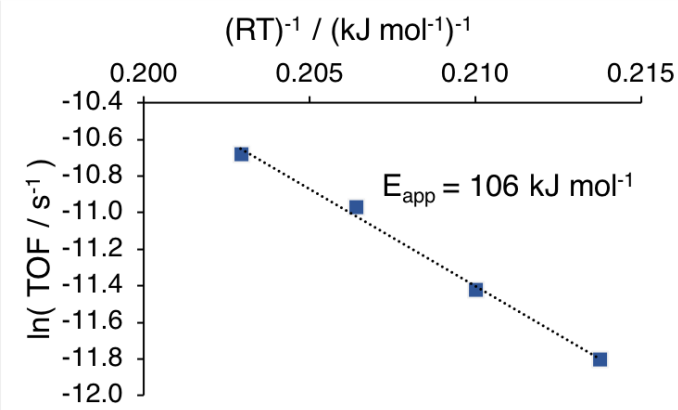

**Figure S9.** Arrhenius plot for ketonization of propanoic acid on ZrOH sites using the free energy pathway of Figure 7. Values of TOF were calculated using the full expression of the energetic span model.[26]

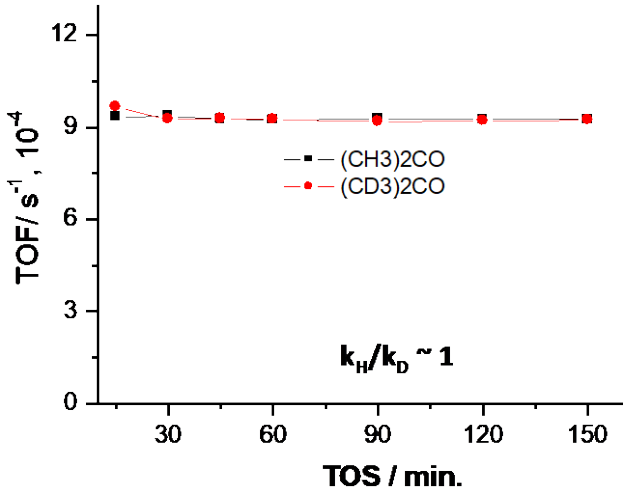


**Figure S10**. Kinetic isotope effect over a 0.1ZrCp/$SiO_2$ catalyst using propan-2-one and deuterated propan-2-one substrate. Reaction conditions: T = 573 K, $P_{Total}$ = 1 atm, $Q_{Total}$ = 100 $cm^3$ $min^{-1}$, $P_{ketone}$ ≈ 0.2 kPa, $M_{Cat}$ = 0.1 g.

## Energetic span model, generalized degrees of rate control and apparent activation energy: aldol condensation

Given the reaction mechanism for aldol condensation depicted in Scheme 3, and assuming negligible product partial pressures under differential conversion, Equation S1 simplifies to

$$\mathrm{TOF} = \frac{k_B T}{h} \frac{P_{\mathrm{ketone}}^2 \, e^{-\Delta G_{\mathrm{rxn}}/RT}}{M} \tag{S13}$$

$$M = P_{\mathrm{ketone}}^2 \left( e^{\frac{G_{\mathrm{D}\ddagger} - G_{\mathrm{C}} - \Delta G_{\mathrm{rxn}}}{RT}} + e^{\frac{G_{\mathrm{C}\ddagger} - G_{C} - \Delta G_{\mathrm{rxn}}}{RT}} \right) + P_{\mathrm{ketone}} \left( e^{\frac{G_{\mathrm{D}\ddagger} - G_{\mathrm{B}} - \Delta G_{\mathrm{rxn}}}{RT}} + e^{\frac{G_{\mathrm{C}\ddagger} - G_{B} - \Delta G_{\mathrm{rxn}}}{RT}} \right) + e^{\frac{G_{\mathrm{D}\ddagger} - G_{\mathrm{A}}}{RT}} + e^{\frac{G_{\mathrm{C}\ddagger} - G_{\mathrm{A}}}{RT}} \tag{S14}$$

The associated generalized degrees of rate controls (following Equation S6) and the apparent activation energy are as follows

$$X_A = -\frac{e^{(G_B+G_C+\Delta G_{rxn})/RT}}{P_{ketone}^2 e^{(G_A+G_B)/RT} + P_{ketone} e^{(G_A+G_C)/RT} + e^{(G_B+G_C+\Delta G_{rxn})/RT}} \quad \text{(S15)}$$

$$X_B = -\frac{P_{ketone} e^{(G_A+G_C)/RT}}{P_{ketone}^2 e^{(G_A+G_B)/RT} + P_{ketone} e^{(G_A+G_C)/RT} + e^{(G_B+G_C+\Delta G_{rxn})/RT}} \quad \text{(S16)}$$

$$X_C = -\frac{P_{ketone}^2 e^{(G_A+G_B)/RT}}{P_{ketone}^2 e^{(G_A+G_B)/RT} + P_{ketone} e^{(G_A+G_C)/RT} + e^{(G_B+G_C+\Delta G_{rxn})/RT}} \quad \text{(S17)}$$

$$X_{C^\ddagger} = \frac{e^{G_{C^\ddagger}/RT}}{e^{G_{C^\ddagger}/RT} + e^{G_{D^\ddagger}/RT}} \quad \text{(S18)}$$

$$X_{D^\ddagger} = \frac{e^{G_{D^\ddagger}/RT}}{e^{G_{C^\ddagger}/RT} + e^{G_{D^\ddagger}/RT}} \quad \text{(S19)}$$

$$E_{app} = RT + X_A H_A^0 + X_B H_B^0 + X_C H_C^0 + X_{C^\ddagger} H_{C^\ddagger}^0 + X_{D^\ddagger} H_{D^\ddagger}^0 \quad \text{(S20)}$$

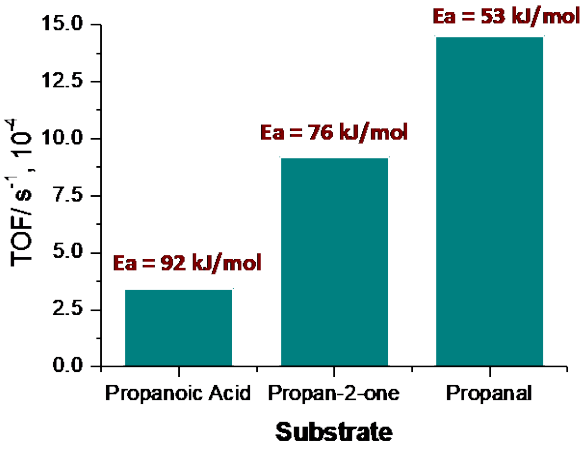


**Figure S11**. Comparison in TOF and activation energy of carboxylic acid, ketone and aldehyde. Reaction conditions: T = 573 K, $P_{Total}$ = 1 atm, $Q_{Total}$ = 100 $cm^3$ $min^{-1}$, $P_{reactant}$ ≈ 0.2 kPa, $M_{Cat}$ = 0.1 g.